Synthetic Models of the Inactive Copper(II)−Tyrosinate and Active Copper(II)−Tyrosyl Radical Forms of Galactose and Glyoxal Oxidases

Jason A. Halfen, Brian A. Jazdzewski, Samiran Mahapatra, Lisa M. Berreau, Elizabeth C. Wilkinson, Lawrence Que, Jr., and William B. Tolman*

Contribution from the Department of Chemistry and Center for Metals in Biocatalysis, University of Minnesota, 207 Pleasant St. SE, Minneapolis, Minnesota 55455

Received January 8, 1997[⊗]

Abstract: A series of Cu^{II} and Zn^{II} complexes with new ligands having either one or two substituted phenolates appended to the 1,4,7-triazacyclononane frame were prepared and characterized by optical absorption, EPR, NMR, and/or resonance Raman spectroscopy, cyclic voltammetry, and, in eight cases, X-ray crystallography. Features of the active site geometries of the Cu^{II}−tyrosinate forms of galactose and glyoxal oxidases (GAO and GLO) were modeled by these complexes, including the binding of a redox-active phenolate and an exogenous ligand (Cl^-, $CH_3CO_2^-$, or CH_3CN) in a *cis*-equatorial position of a square pyramidal metal ion. The role of the unique *ortho* S−C covalent bond between a cysteine (C228) and the equatorial tyrosinate (Y272) in the proteins was probed through an examination of the optical absorption and electrochemical properties of sets of similar complexes comprised of phenolate ligands with differing *ortho* substituents, including thioether groups. The *o*-alkylthio unit influences the $PhO^- \rightarrow Cu^{II}$ LMCT transition and the M^{II}−phenolate/M^{II}−phenoxyl radical redox potential, but to a relatively small degree. Electrochemical and chemical one-electron oxidations of the Cu^{II} and Zn^{II} complexes of ligands having *tert*-butyl protecting groups on the phenolates yielded new species that were identified as novel M^{II}−phenoxyl radical compounds analogous to the active Cu^{II}−tyrosyl radical forms of GAO and GLO. The M^{II}−phenoxyl radical species were characterized by optical absorption, EPR, and resonance Raman spectroscopy, as well as by their stoichiometry of formation and chemical reduction. Notable features of the Cu^{II}−phenoxyl radical compounds that are similar to their protein counterparts include EPR silence indicative of magnetic coupling between the Cu^{II} ion and the bound radical, a band with $\lambda_{max} \approx 410$ nm ($\epsilon \approx 3900$ M^{-1} cm^{-1}) in UV−vis spectra diagnostic for the phenoxyl radical, and a feature attributable to the phenoxyl radical C−O vibration (ν_{7a}) in resonance Raman spectra. Similar Raman spectra and electrochemical behavior for the Zn^{II} analogs, as well as an isotropic signal at $g = 2.00$ in their X-band EPR spectra, further corroborate the formulations of the M^{II}−phenoxyl radical species.

Introduction

The copper-containing metalloenzymes galactose oxidase (GAO)[1] and glyoxal oxidase (GLO)[2] from fungi perform the two-electron oxidations of primary alcohols or aldehydes, respectively, coupled with the reduction of O_2 to H_2O_2 (eqs 1 and 2). These enzymes are unusual because, in contrast to most

$$\text{GAO:}\quad RCH_2OH + O_2 \rightarrow RCHO + H_2O_2 \qquad (1)$$

$$\text{GLO:}\quad RCHO + H_2O + O_2 \rightarrow RCO_2H + H_2O_2 \qquad (2)$$

copper proteins that effect multielectron redox reactions by using multinuclear active sites (i.e., 1 e^- per Cu, shuttling between Cu^I and Cu^{II}),[3] GAO and GLO use an isolated, monocopper center to carry out two-electron redox chemistry. Details of the geometry of this center in GAO have been revealed by X-ray crystallography (Figure 1).[4] The copper ion is square pyramidal, with a tyrosinate ligand (or protonated form) weakly bound in the axial position and two histidine imidazoles, a second tyrosinate, and either H_2O (pH 7.0) or acetate (from buffer, pH 4.5) in the equatorial sites. Interestingly, the equatorial tyrosinate is linked to a nearby cysteine via an *ortho* C−S bond to afford a thioether-modified phenolate ligand (Y272−C228), which is within π-stacking distance of a tryptophan residue (not shown). Spectroscopic studies of GAO and GLO indicate that the isolated inactive enzyme contains a Cu^{II}−tyrosinate fragment (*inactive*, Figure 2) which upon treatment with oxidants yields the functionally competent form *(active)* consisting of a novel

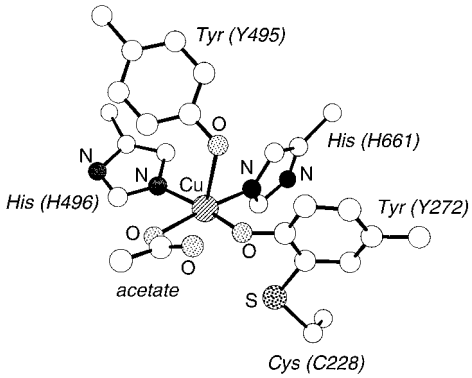

Figure 1. Drawing of the active site of galactose oxidase at pH 4.5 as determined by X-ray crystallography (ref 4).

[⊗] Abstract published in *Advance ACS Abstracts,* August 1, 1997.

(1) (a) Whittaker, J. W. In *Metalloenzymes Involving Amino Acid Residue and Related Radicals*; Sigel, H., Sigel, A., Eds.; Marcel Dekker: New York, 1994; Vol. 30, pp 315−360. (b) Knowles, P. F.; Ito, N. *Perspectives in Bio-inorganic Chemistry*; Jai Press Ltd.: London, 1994; Vol. 2, pp 207−244. (c) Whittaker, J. W. In *Bioinorganic Chemistry of Copper*; Karlin, K. D., Tyeklár, Z., Eds.; Chapman & Hall, Inc.: New York, 1993; pp 447−458.

(2) Whittaker, M. M.; Kersten, P. J.; Nakamura, N.; Sanders-Loehr, J.; Schweizer, E. S.; Whittaker, J. W. *J. Biol. Chem.* **1996**, *271*, 681−687.

(3) (a) Solomon, E. I.; Baldwin, M. J.; Lowery, M. D. *Chem. Rev.* **1992**, *92*, 521−542. (b) Solomon, E. I.; Sundaram, U. M.; Machonkin, T. E. *Chem. Rev.* **1996**, *96*, 2563−2605.

(4) (a) Ito, N.; Phillips, S. E. V.; Stevens, C.; Ogel, Z. B.; McPherson, M. J.; Keen, J. N.; Yadav, K. D. S.; Knowles, P. F. *Nature* **1991**, *350*, 87−90. (b) Ito, N.; Phillips, S. E. V.; Stevens, C.; Ogel, Z. B.; McPherson, M. J.; Keen, J. N.; Yadav, K. D. S.; Knowles, P. R. *Faraday Discuss.* **1992**, *93*, 75−84. (c) Ito, N.; Phillips, S. E. V.; Yadav, K. D. S.; Knowles, P. F. *J. Mol. Biol.* **1994**, *238*, 794−814.

S0002-7863(97)00066-8 CCC: $14.00

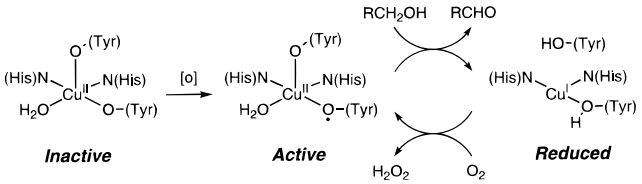

Figure 2. Active site forms and catalytic mechanism postulated for galactose oxidase (refs 1, 4, and 5−7).

Cu^{II}−radical pair in the active site, with the radical localized on the equatorial, covalently modified tyrosinate ligand.[1,2,5,6] Key supporting evidence for this hypothesized formulation includes EPR silence attributed to antiferromagnetic coupling between the two $S = 1/2$ centers, X-ray absorption edge data indicative of the presence of Cu^{II}, resonance Raman data showing diagnostic phenoxyl radical vibrations, and intense optical absorption bands, including one with $\lambda_{max} = 444$ nm ($\epsilon = 5194\ M^{-1}\ cm^{-1}$, GAO) that is postulated to be due in part to a $\pi \rightarrow \pi^*$ transition of the phenoxyl radical. The ability of the mononuclear active site to carry out two-electron redox chemistry has been rationalized by invoking cycling between this unique Cu^{II}−tyrosyl radical unit (*active*, Figure 2) and a Cu^{I} state *(reduced)*, with the Cu^{II}−tyrosyl radical form being directly responsible for hydrogen atom abstraction from the substrate bound in the equatorial position adjacent to Y272 during turnover.[1,4,6,7]

The unusual nature of the cysteine-modified Cu^{II}−tyrosyl radical species, its critical functional role in enzyme catalysis, and the provocative mechanisms proposed to explain how it oxidizes substrates provide ample impetus for undertaking in-depth studies of the properties of synthetic analogs of the GAO and GLO active sites. Further rationale for study derives from recognition of the Cu^{II}−tyrosyl radical species in these enzymes as interesting members of a growing class of functionally important metal−radical arrays in proteins that delocalize multiple oxidizing equivalents in a manner complementary to those involving polynuclear metal-containing active sites.[8] Previous synthetic modeling efforts primarily have focused on Cu^{II}−phenolate complexes akin to the inactive state of the enzyme.[9] Ligands with (methylthio)phenolate donors also have been used in order to more closely mimic the cysteine-modified tyrosinate in the proteins, but accurate mononuclear model complexes and derived metal−phenoxyl radical species supported by these ligands have been elusive.[10] Well-characterized metal complexes with proximate or directly bonded phenoxyl radicals are rare;[11] notable examples are Lippard's monozinc(II) and diiron(III) compounds with pendant, uncoordinated radicals[12] and Wieghardt's phenoxyl radicals coordinated to tri- and tetravalent metals (Fe^{III}, Ga^{III}, Mn^{III}, Mn^{IV}, and Cr^{III}; structurally characterized for Cr^{III}) derived from the oxidation of complexes of 1,4,7-tris(phenolato)-1,4,7-triazacyclononanes.[13]

We report herein our progress toward the synthesis and structural and spectroscopic characterization of models of GAO and GLO active site species. We have elucidated the properties of new mono- and bis(phenolato)copper(II) and -zinc(II) complexes relevant to the inactive form of the enzymes, with a particular view toward evaluating the spectroscopic and redox influences of phenolate ring substituents, including alkylthio groups that mimic the enzyme cysteine modification. In addition, we have prepared via electrochemical and chemical means several oxidized versions which, on the basis of spectroscopic and other evidence, we assign as novel metal−phenoxyl radical species analogous to the active enzyme form (Figure 2).[14] Portions of this work have been communicated previously.[15]

Results and Discussion

A. Cu^{II}− and Zn^{II}−Phenolate Complexes. Synthesis. In order to replicate key features of the active site environment of GAO and GLO, we designed a series of chelates that would favor monomeric square pyramidal Cu^{II} geometries, provide one phenolate donor in an equatorial position for eventual oxidation to a phenoxyl radical, and be amenable to adjustment of steric and electronic influences in order to tune the spectroscopic and redox properties of derived complexes and enhance the stability of metal-phenoxyl radical species. The chosen ligands $HL^{RR'}$ (Scheme 1, where R and R′ refer to the substituents *para* and *ortho* to the phenolic oxygen atom, respectively)[16] were isolated as crystalline solids in good to excellent yields from the reaction of the Mannich base l-(hydroxymethyl)-4,7-diisopropyl-1,4,7-triazacyclononane (produced in situ from the reaction of 1,4-diisopropyl-1,4,7-triazacyclononane[17] and aqueous formaldehyde) with 2,4-disubstituted phenols in refluxing methanol.

(5) (a) Baron, A. J.; Stevens, C.; Wilmot, C.; Seneviratne, K. D.; Blakeley, V.; Dooley, D. M.; Phillips, S. E.; Knowles, P. F.; McPherson, M. J. *J. Biol. Chem.* **1994**, *269*, 25095−25105. (b) Knowles, P. F.; Brown, R. D., III; Koenig, S. H.; Wang, S.; Scott, R. A.; McGuirl, M. A.; Brown, D. E.; Dooley, D. M. *Inorg. Chem.* **1995**, *34*, 3895−3902.

(6) Clark, K.; Penner-Hahn, J. E.; Whittaker, M. M.; Whittaker, J. W. *J. Am. Chem. Soc.* **1990**, *112*, 6433−6434.

(7) (a) Branchaud, B. P.; Montague-Smith, M. P.; Kosman, D. J.; McLaren, F. R. *J. Am. Chem. Soc.* **1993**, *1l5*, 798−800. (b) Wachter, R. M.; Branchaud, B. P. *J. Am. Chem. Soc.* **1996**, *118*, 2782−2789. (c) Wachter, R. M.; Branchaud, B. P. *Biochemistry* **1996**, *35*, 14425−14435.

(8) (a) *Metalloenzymes Involving Amino Acid Residue and Related Radicals;* Sigel, H., Sigel, A., Eds.; Marcel Dekker: New York, 1994; Vol. 30. (b) Stubbe, J. A. *Annu. Rev. Biochem.* **1989**, *58*, 257−285. (c) Pedersen, J. Z.; Finazzi-Agro, A. *FEBS Lett.* **1993**, *325*, 53−58. (d) Fontecave, M.; Pierre, J. L. *Bull. Soc. Chim. Fr.* **1996**, *133*, 653−660.

(9) (a) Kitajima, N.; Whang, K.; Moro-oka, Y.; Uchida, A.; Sasada, Y. *J. Chem. Soc., Chem. Commun.* **1986**, 1504−1505. (b) Rajendran, U.; Viswanathan, R.; Palaniandavar, M.; Lakshminarayanan, M. J. *Chem. Soc., Dalton Trans.* **1992**, 3563−3564. (c) Uma, R.; Viswanathan, R.; Palaniandavar, M.; Lakshminarayanan, M. *J. Chem. Soc., Dalton Trans.* **1994**, 1219−1226. (d) Adams, H.; Bailey, N. A.; Fenton, D. E.; He, Q. *Inorg. Chim. Acta* **1994**, *215*, 1−3. (e) Adams, H.; Bailey, N. A.; de Barbarin, C. O. R.; Fenton, D. E.; He, Q.-Y. *J. Chem. Soc., Dalton Trans.* **1995**, 2323−2331. (f) Shulz, D.; Weyhermuller, T.; Wieghardt, K.; Butzlaff, C.; Trautwein, A. X. *Inorg. Chim. Acta* **1996**, *246*, 387−394. (g) Karlin, K. D.; Cohen, B. I.; Hayes, J. C.; Farooq, A.; Zubieta, J. *Inorg. Chem.* **1987**, *26*, 147- 153.

(10) (a) Whittaker, M.; Chuang, Y.; Whittaker, J. *J. Am. Chem. Soc.* **1993**, *115*, 10029−10035. (b) Whittaker, M. M.; Duncan, W. R.; Whittaker, J. W. *Inorg. Chem.* **1996**, 35, 382−386.

(11) Goldberg, D. P.; Lippard, S. J. In *Mechanistic Bioinorganic Chemistry;* Thorp, H. H., Pecoraro, V. L., Eds.; American Chemical Society: Washington, DC, 1995; Adv. Chem. Ser. Vol. 246, pp 61−81.

(12) (a) Goldberg, D. P.; Watton, S. P.; Masschelein, A.; Wimmer, L.; Lippard, S. J. *J. Am. Chem. Soc.* **1993**, *115*, 5346−5347. (b) Goldberg, D. P.; Koulougliotis, D.; Brudvig, G. W.; Lippard, S. J. *J. Am. Chem. Soc.* **1995**, *117*, 3134−3144.

(13) (a) Hockertz, J.; Steenken, S.; Wieghardt, K.; Hildebrandt, P. *J. Am. Chem. Soc.* **1993**, *115*, 11222−11230. (b) Sokolowski, A.; Bothe, E.; Bill, E.; Weyhermuller, T.; Wieghardt, K. *J. Chem. Soc., Chem. Commun.* **1996**, 1671−1672. (c) Adam, B.; Bill, E.; Bothe, E.; Goerdt, B.; Haselhorst, G.; Hildenbrand, K.; Sokolowski, A.; Steenken, S.; Weyhermüller, T.; Wieghardt, K. *Chem. Eur. J.* **1997**, *3*, 308−319.

(14) Since the initial submission of this manuscript, several reports of the oxidation chemistry of Cu^{II}−phenolate complexes have appeared: (a) Wang, Y.; Stack, T. D. P. *J. Am. Chem. Soc.* **1996**, *118*, 13097−13098. (b) Zurita, D.; Gautier-Luneau, I.; Ménage, S.; Pierre, J.-L.; Saint-Aman, E. *J. Biol. Inorg. Chem.* **1997**, *2*, 46−55. (c) Zurita, D.; Scheer, C.; Pierre, J.-L.; Saint-Aman, E. *J. Chem. Soc., Dalton Trans.* **1996**, 4331−4336. (d) Itoh, S.; Takayama, S.; Arakawa, R.; Furuta, A.; Komatsu, M.; Ishida, A.; Takamuku, S.; Fukuzumi, S. *Inorg. Chem.* **1997**, 36, 1407−1416.

(15) Halfen, J. A.; Young, V. G., Jr.; Tolman, W. B. *Angew. Chem., Int. Ed. Engl.* **1996**, *35*, 1687−1690.

(16) Related monophenolate 1,4,7-triazacyclononane ligands with additional N-bound carboxylates have been examined: Stockheim, C.; Hoster, L.; Weyhermüller, T.; Wieghardt, K.; Nuber, B. *J. Chem. Soc., Dalton Trans.* **1996**, 4409−4416.

(17) (a) Houser, R. P.; Halfen, J. A.; Young, V. G., Jr.; Blackburn, N. J.; Tolman, W. B. *J. Am. Chem. Soc.* **1995**, *117*, 10745−10746. (b) Mahapatra, S.; Halfen, J. A.; Wilkinson, E. C.; Pan, G.; Wang, X.; Young, V. G., Jr.; Cramer, C. J.; Que, L., Jr.; Tolman, W. B. *J. Am. Chem. Soc.* **1996**, *118*, 11555−11574.

Scheme 1

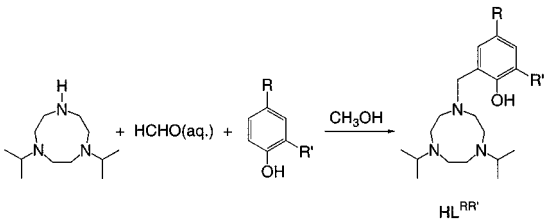

Phenol Substitution Pattern	*Ligand ($L^{RR'}$)*	*Yield*
R = R' = CH_3	L^{Me2}	71%
R = R' = $C(CH_3)_3$	L^{tBu2}	90%
R = CH_3, R' = OCH_3	L^{MeOMe}	63%
R = CH_3, R' = SCH_3	L^{MeSMe}	70%
R = $C(CH_3)_3$, R' = SCH_3	L^{tBuSMe}	55%

Scheme 2

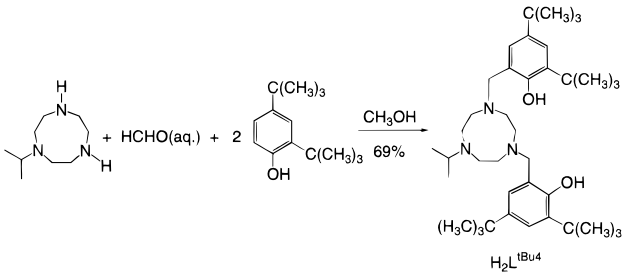

Similar methods were used previously for the preparation of 1,4,7-tris(phenol)-1,4,7-triazacyclononane ligands,[13b,c,18,19] as well as mono(phenol)-appended bis(pyridylmethyl)amine tripods.[20] The ligands HL^{MeSMe} and HL^{tBuSMe} with alkylthio appendages akin to the cysteine-modified tyrosinate ligand Y272−C228 in the proteins were constructed from the appropriate 4-alkyl-2-(alkylthio)phenols (alkyl = methyl, *tert*-butyl). These were prepared by the reaction of the parent 4-alkylphenols with chlorodimethylsulfonium bisulfate in H_2SO_4 followed by hydrolysis of the intermediate aryldimethylsulfonium salt.[21] Finally, in order to more closely model the bis(tyrosinate) ligation in the proteins, a second class of ligands with two phenolate arms was designed. We have prepared one example so far, $H_2L^{tBu_4}$ (Scheme 2), by the Mannich base procedure described above, but starting with the new synthon 1-isopropyl-1,4,7-triazacyclononane, which was constructed via an alkylation/deprotection sequence from 1,4-ditosyl-1,4,7-triazacyclononane.[22]

A series of crystalline Cu^{II} and Zn^{II} complexes of the new monophenolate ligands $L^{RR'}$ was prepared by deprotonation of the phenols $HL^{RR'}$ with NaH in THF followed by treatment with the appropriate anhydrous metal salts (Scheme 3); $H_2L^{tBu_4}$ similarly was converted to $L^{tBu_4}M$ (M = Cu, Zn). Attempts to prepare Cu^{I} complexes by treating the deprotonated ligands with CuCl or $[Cu(CH_3CN)_4]ClO_4$ generally failed due to disproportionation reactions, as indicated by the purple color of the solutions (due to Cu^{II}−phenolate species) and the presence of colloidal copper metal.

X-ray Crystal Structures. We have solved the X-ray crystal structures of eight complexes of the new ligands; of these, crystallographic data for five (data for $L^{Me_2}CuCl$ were reported previously)[15] and selected bond distances and angles for six are listed in Tables 1 and 2, respectively. A representative subset of five structural drawings is shown in Figure 3. Complete data for all structures are provided in the Supporting Information.

Scheme 3

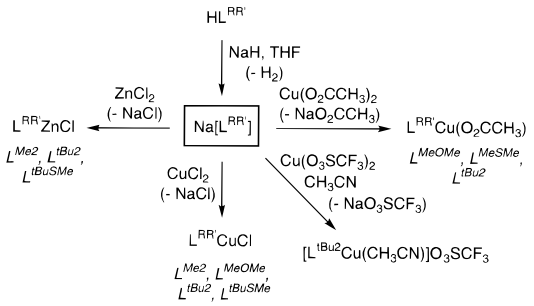

All of the structures verify binding of all available donor atoms in the ligands to the metal ion to yield mononuclear complexes, which for the monophenolate cases also contain a fifth exogenous ligand (Cl^-, $CH_3CO_2^-$, or CH_3CN). The Cu^{II} compounds of the monophenolate chelates (typified by the structures in Figure 3a,c,d) are best described as square pyramidal, with the phenolate and exogenous groups occupying *cis*-equatorial positions; the maximum τ value[23] is 0.27 [$L^{MeOMe}Cu(O_2CCH_3)$; see the Supporting Information]. As reported previously for other monomeric Cu^{II}−phenolate complexes,[9,19a] the $Cu-O_{phenolate}$ bond is relatively short [av 1.92 Å, range 1.904(5)−1.947(3) Å] and induces by a *trans* influence lengthening of the opposite Cu−N bond (e.g., for $L^{Me_2}CuCl$, Cu−N4 is longer by 0.08 Å than the other $Cu-N_{eq}$ distance).

Comparison of the pairs of structures $L^{Me_2}MCl$ (M = Cu or Zn, Figure 3a,b) and $L^{tBu_4}M$ (M = Cu or Zn, only shown for M = Cu in Figure 3e) reveals the consequences of coordination of the same ligand in complexes different only with respect to the nature of the metal ion. Whereas $L^{Me_2}CuCl$ is square pyramidal ($\tau = 0.07$), $L^{Me_2}ZnCl$ is distorted trigonal bipyramidal ($\tau = 0.61$) with the phenolate and two amine donors (Nl and N4) comprising the trigonal plane and the third amine N-atom (Nl) and Cl^- residing in pseudoaxial positions. On the other hand, the structures of $L^{tBu_4}M$ (M = Cu or Zn) are more similar, with each best described as having metal ion geometries intermediate between square pyramidal and trigonal bipyramidal (Cu, $\tau = 0.45$; Zn, $\tau = 0.60$). Both contain a MeOH solvate molecule that is hydrogen-bonded to the O-donor atom of one of the coordinated phenolates. The structure of $L^{tBu_4}Cu$ is quite similar to that reported for a Cu^{II} complex of a tris(phenolato)-1,4,7-triazacyclononane ligand, except for the presence of a dangling, uncoordinated phenol in the latter.[19a] The bis(tyrosinate) ligation present in the GAO and GLO active sites is modeled by these compounds insofar as they also have two phenolates in symmetry inequivalent positions, although the distinct long axial/short equatorial phenolate bonding pattern for the square pyramidal copper center in the proteins is not replicated in the synthetic complexes. We cannot provide a definitive rationale for the significant difference between the Cu/Zn pair of structures for the L^{Me_2} case compared to the lesser divergence seen for L^{tBu_4}, although we surmise that the steric hindrance due to the phenolate *tert*-butyl groups in the latter is an important factor.

The structure of the GAO active site crystallographically characterized at pH 4.5 (Figure 1)[4] is most closely modeled by $L^{MeSMe}Cu(O_2CCH_3)$ (Figure 3c), which contains phenolate and acetate ligands bound in *cis*-equatorial positions to a distorted square pyramidal Cu^{II} ion ($\tau = 0.24$). The acetate coordination

(18) Moore, D. A.; Fanwick, P. E.; Welch, M. J. *Inorg. Chem.* **1989**, *28*, 1504−1506.
(19) (a) Auerbach, U.; Eckert, U.; Wieghardt, K.; Nuber, B.; Weiss, J. *Inorg. Chem.* **1990**, *29*, 938−944. (b) Auerbach, U.; Weyhermuller, T.; Wieghardt, K.; Nuber, B.; Brill, E.; Butzlaff, C.; Trautwein, A. X. *Inorg. Chem.* **1993**, *32*, 508−519.
(20) Cox, D. D.; Que, L., Jr. *J. Am. Chem. Soc.* **1988**, *110*, 8085−8092.
(21) Pilgram, K. H.; Medema, D.; Soloway, S. B.; Gaertner, G. W. U.S. Patent 3772391, 1973.
(22) Sessler, J. L.; Sibert, J. W.; Lynch, V. *Inorg. Chem.* **1990**, *29*, 4143−4146.
(23) Addison, A. W.; Rao, T. N.; Reedijk, J.; von Rijn, J.; Verschoor, G. C. *J. Chem. Soc., Dalton Trans.* **1984**, 1349−1356.

Table 1. Summary of X-ray Crystallographic Data[a]

complex	$[L^{Me_2}ZnCl]\cdot 0.32H_2O$	$[L^{MeSMe}Cu(O_2CCH_3)]\cdot CH_2Cl_2$	$[L^{tBu_2}Cu(CH_3CN)]\cdot CF_3SO_3\cdot C_7H_8$	$[L^{tBu_4}Cu]\cdot CH_3OH$	$[L^{tBu_4}Zn]\cdot CH_3OH$
empirical formula	$C_{21}H_{36.64}N_3O_{1.32}ClZn$	$C_{24}H_{41}N_3O_3SCl_2Cu$	$C_{37}H_{59}N_4O_4F_3SCu$	$C_{40}H_{67}N_3O_3Cu$	$C_{40}H_{67}N_3O_3Zn$
formula weight	452.51	568.10	776.48	701.51	703.34
crystal system	monoclinic	monoclinic	triclinic	monoclinic	monoclinic
space group	$P2_{1/c}$	$P2_1/n$	$P\bar{1}$	$P2_1/c$	$P2_1/n$
a (Å)	12.746(3)	12.676(3)	11.798(2)	13.5373(5)	16.952(3)
b (Å)	12.911(3)	13.228(3)	14.084(4)	10.4219(4)	11.435(2)
c (Å)	13.648(3)	17.457(4)	15.065(2)	29.190(1)	21.492(4)
α (deg)			73.74(3)		
β (deg)	90.36(3)	102.29(3)	67.52(3)	102.396(1)	94.70(3)
γ (deg)			65.97(3)		
V (Å^3)	2245.9(8)	2860(1)	2089.5(7)	4022.3(3)	4152(1)
Z	4	4	2	4	4
density(calcd) (g cm^{-3})	1.338	1.361	1.234	1.158	1.127
temp (K)	293(2)	293(2)	293(2)	173(2)	293(2)
crystal size (mm)	0.50 × 0.35 × 0.25	0.45 × 0.40 × 0.30	0.50 × 0.45 × 0.10	0.50 × 0.15 × 0.08	0.45 × 0.37 × 0.35
diffractometer	Enraf-Nonius CAD-4	Enraf-Nonius CAD-4	Enraf-Nonius CAD-4	Siemens SMART	Enraf-Nonius CAD-4
abs coeff (mm^{-1})	1.230	1.053	0.626	0.581	0.628
2θ max (deg)	50.00	49.98	50.04	50.06	50.00
no. of reflections collected	4131	5252	7717	19943	7289
no. of indep reflections	3942	5009	7325	7059	4255
no. of reflections with $I > 2\sigma(I)$	2610	3013	3670	4750	2689
no. of variable parameters	258	307	416	504	454
R_1/wR_2[b]	0.0460/0.1058	0.0606/0.1410	0.0758/0.1648	0.0507/0.1159	0.0496/0.1017
goodness of fit (F^2)	1.021	1.021	1.042	1.001	1.046
largest diff features (e$^-$ Å^{-3})	0.363/−0.362	0.542/−0.823	0.476/−0.503	0.709/−0.631	0.192/−0.183

[a] Radiation used: Mo Kα (λ = 0.071 073 Å). [b] $R_1 = \sum||F_o| - |F_c||/\sum|F_o|$; $wR_2 = [\sum[w(F_o^2 - F_c^2)^2]]^{1/2}$, where $w = 1/\sigma^2(F_o^2) + (aP)^2 + bP$.

borders on asymmetric bidentate,[24] the oxygen atom O3 being directly *trans* to the axial amine N-donor (N3; the N3-Cu1−O3 angle is 173°) with an O3···Cu1 distance of 2.72 Å. This weak axial interaction of a Cu^{II} ion with a carbonyl oxygen atom resembles that observed in $[L^{iPr_3}Cu(O_2CCH_3)_2]$ (L^{iPr_3} = 1,4,7-triisopropyl-1,4,7-triazacyclononane; $N_{axial}-Cu-O_{acetate}$ = 156°; $Cu\cdots O_{acetate}$ = 3.15 Å)[25] and some type 1 copper proteins.[26] The thiomethyl S-atom (Sl) does not coordinate to the Cu^{II} ion [Cul···Sl = 4.606(2) Å] in contrast to the structures of other Cu^{II} complexes containing *o*-thioether-substituted phenolate ligands.[10a] An additional noteworthy structural feature is the conformation of this thiomethyl substituent, which is coplanar with the phenolate ring [the C14−C13−Sl−C17 torsion angle is −0.3(6)°]. This resembles the conformation of the redox-active Y272−C228 pair in galactose oxidase in which S^γ and C^β of Cys228 are coplanar with the phenolic ring of Y272, an observation which led to the proposal that the $S_{Cys}-C_{Tyr}$ bond possesses partial double bond character.[4b] In $L^{MeSMe}Cu(O_2CCH_3)$ the $C_{arene}-S$ distance is 1.767(6) Å, which is typical for such distances in thioether-substituted arenes argued to have little double bond character.[27] In addition, a structure similar to that of $L^{MeSMe}Cu(O_2CCH_3)$ was found for the L^{MeOMe} analog (see the Supporting Information). The finding of identical conformations of the *o*-OMe and -SMe groups suggests that intermolecular packing forces govern the conformations of these side chains and that unique S−C multiple bonding need not be invoked to explain the planarity of the *o*-(methylthio)phenolate.

Spectroscopic Properties. Spectroscopic characterization of the Cu^{II}− and Zn^{II}−phenolate complexes was undertaken in order to correlate their solution structures with those determined by X-ray crystallography and to understand the electronic influences of the phenolate substituents, in particular the alkylthio groups akin to the enzyme C228 appendage. The diamagnetic Zn^{II} complexes exhibit sharp ^{1}H NMR spectra with increases in the number and multiplicity of the macrocycle backbone methylene resonances compared to the free ligand that are diagnostic for metal ion binding.[25] Despite the inequivalence of the phenolate dispositions in the X-ray structure of $L^{tBu_4}Zn$, only a single set of resonances appears in the NMR spectrum, suggestive of the operation of a fluxional process in solution that rapidly interchanges the phenolate environments. All of the Cu^{II} complexes exhibit axial signals in their X-band EPR spectra (frozen solutions at 77 K) that are consistent with a $d_{x^2-y^2}$ ground state ($g_{||} > g_\perp > 2.0$, $A_{||} \approx 150-170$ G) with a minor rhombic perturbation (perhaps indicative of a distortion toward a trigonal bipyramidal structure) that is most clearly resolved in the acetate and azide complexes. The Cu^{II} complexes are also deeply colored due to absorption features with $\lambda_{max} \approx 450-530$ nm ($\epsilon \approx 1000-2000$ M^{-1} cm^{-1}) that we assign as $PhO^- \rightarrow Cu^{II}$ ligand-to-metal charge transfer (LMCT) transitions by analogy to other known Cu^{II}−phenolate systems (Table 3 and Figure 4).[9] This assignment is supported by Raman spectroscopic studies of $[L^{tBu_2}Cu(CH_3CN)]CF_3SO_3$ and $L^{tBu_4}Cu$, which show resonance-enhanced phenolate vibrational features upon irradiation into the absorption band *(vide infra).* Also consistent with the LMCT attribution, comparison of the λ_{max} values for the isostructural series $L^{RR'}Cu(O_2CCH_3)$ and $L^{RR'}CuCl$ (Table 3) shows that the energy of the transition within each series increases (λ_{max} decreases) as the energy of the filled ligand-based orbitals decreases according to the order L^{MeOMe} (most electron rich) ≈ L^{MeSMe} ≈ L^{tBuSMe} > L^{Me_2} ≈ L^{tBu_2} (least electron rich). The overall range of energies within each series is not large, however, which by extrapolation implies a relatively minor role for the thioether appendage in tuning the redox properties of the equatorial tyrosinate in GAO and GLO. This conclusion is further corroborated by the results of cyclic voltammetry experiments (*vide infra*). The LMCT feature in $L^{tBu_4}Cu$ (Figure 4) is shifted significantly to higher energy compared to the monophenolate compounds, consistent with greater electron density at the Cu^{II} ion and raised acceptor orbital energies due to the second phenolate donor.

(24) Rardin, R. L.; Tolman, W. B.; Lippard, S. J. *New J. Chem.* **1991**, *15*, 417−430.

(25) Halfen, J. A.; Mahapatra, S.; Wilkinson, E. C.; Gengenbach, A. J.; Young, V. G., Jr.; Que, L., Jr.; Tolman, W. B. *J. Am. Chem. Soc.* **1996**, *118*, 763−776.

(26) Adman, E. T. *Adv. Protein Chem.* **1991**, *42*, 145−197.

(27) (a) Peach, M. E.; Burschka, C. *Can. J. Chem.* **1982**, *60*, 2029−2037. (b) Blackmore, W. R.; Abrahams, S. C. *Acta Crystallogr.* **1955**, *8*, 329−335. (c) Cox, E. G.; Gillot, R. J. J. H.; Jeffrey, G. A. *Acta Crystallogr.* **1949**, *2*, 356−363.

Table 2. Selected Bond Lengths (Å) and Angles (deg) for Complexes Characterized by X-ray Crystallography[a]

	$L^{Me_2}CuCl$		
Cu(1)−O(1)	1.916(5)	Cu(1)−N(1)	2.069(5)
Cu(1)−N(4)	2.148(6)	Cu(1)−N(7)	2.291(6)
Cu(1)−Cl(1)	2.286(2)	O(1)−Cu(1)−N(1)	92.8(2)
O(1)−Cu(1)−N(4)	167.4(2)	O(1)−Cu(1)−N(7)	109.3(2)
O(1)−Cu(1)−Cl(1)	90.3(2)	N(1)−Cu(1)−N(4)	83.0(2)
N(1)−Cu(1)−N(7)	83.9(3)	N(1)−Cu(1)−Cl(1)	171.4(2)
N(4)−Cu(1)−N(7)	82.2(2)	N(4)−Cu(1)−Cl(1)	92.4(2)
N(7)−Cu(1)−Cl(1)	102.7(2)		
	$[L^{Me_2}ZnCl]\cdot 0.32H_2O$		
Zn(1)−O(1)	1.931(3)	Zn(1)−N(1)	2.316(3)
Zn(1)−N(4)	2.156(4)	Zn(1)−N(7)	2.134(3)
Zn(1)−Cl(1)	2.3410(13)	O(1)−Zn(1)−N(1)	86.86(11)
O(1)−Zn(1)−N(4)	137.63(13)	O(1)−Zn(1)−N(7)	130.34(14)
O(1)−Zn(1)−Cl(1)	95.94(9)	N(1)−Zn(1)−N(4)	79.25(12)
N(1)−Zn(1)−N(7)	80.03(12)	N(1)−Zn(1)−Cl(1)	174.19(10)
N(4)−Zn(1)−N(7)	86.51(14)	N(4)−Zn(1)−Cl(1)	95.31(10)
N(7)−Zn(1)−Cl(1)	101.82(10)		
	$[L^{MeSMe}Cu(O_2CCH_3)]\cdot CH_2Cl_2$		
Cu(1)−O(1)	1.943(4)	Cu(1)−O(2)	1.958(4)
Cu(1)−N(1)	2.046(4)	Cu(1)−N(4)	2.170(5)
Cu(1)−N(7)	2.295(5)	O(2)−C(25)	1.267(7)
O(3)−C(25)	1.236(7)	O(1)−Cu(1)−O(2)	91.6(2)
O(1)−Cu(1)−N(1)	93.4(2)	O(1)−Cu(1)−N(4)	175.5(2)
O(1)−Cu(1)−N(7)	93.7(2)	N(1)−Cu(1)−N(4)	84.1(2)
N(1)−Cu(1)−N(7)	82.8(2)	N(1)−Cu(1)−O(2)	161.3(2)
N(4)−Cu(1)−N(7)	82.4(2)	N(4)−Cu(1)−O(2)	91.9(2)
N(7)−Cu(1)−O(2)	114.8(2)	Cu(1)−O(2)−C(25)	109.5(4)
	$[L^{tBu_2}Cu(CH_3CN)]CF_3SO_3\cdot C_7H_8$		
Cu(1)−O(1)	1.904(4)	Cu(1)−N(10)	2.011(6)
Cu(1)−N(1)	2.017(5)	Cu(1)−N(4)	2.297(5)
Cu(1)−N(7)	2.075(5)	O(1)−Cu(1)−N(10)	82.4(2)
O(1)−Cu(1)−N(1)	94.2(2)	O(1)−Cu(1)−N(4)	106.5(2)
O(1)−Cu(1)−N(7)	169.9(2)	N(1)−Cu(1)−N(4)	84.8(2)
N(1)−Cu(1)−N(7)	86.0(2)	N(1)−Cu(1)−N(10)	164.2(2)
N(4)−Cu(1)−N(7)	83.6(2)	N(4)−Cu(1)−N(10)	111.0(2)
N(7)−Cu(1)−N(10)	94.7(2)	Cu(1)−N(10)−C(25)	158.4(6)
	$[L^{tBu_4}Cu]\cdot CH_3OH$		
Cu(1)−O(1)	1.935(2)	Cu(1)−O(2)	1.916(2)
Cu(1)−N(1)	2.076(2)	Cu(1)−N(2)	2.043(2)
Cu(1)−N(3)	2.363(2)	O(1)−Cu(1)−O(2)	89.45(9)
O(1)−Cu(1)−N(1)	94.17(9)	O(1)−Cu(1)−N(2)	150.85(9)
O(1)−Cu(1)−N(3)	126.49(8)	N(1)−Cu(1)−N(2)	85.26(9)
N(1)−Cu(1)−N(3)	80.29(9)	N(1)−Cu(1)−O(2)	178.12(10)
N(2)−Cu(1)−N(3)	82.22(9)	N(2)−Cu(1)−O(2)	94.17(9)
N(3)−Cu(1)−O(2)	101.42(9)		
	$[L^{tBu_4}Zn]\cdot CH_3OH$		
Zn(1)−O(1)	1.946(3)	Zn(1)−O(2)	1.962(3)
Zn(1)−N(1)	2.244(4)	Zn(1)−N(2)	2.110(5)
Zn(1)−N(3)	2.177(5)	O(1)−Zn(1)−O(2)	92.15(14)
O(1)−Zn(1)−N(1)	89.5(2)	O(1)−Zn(1)−N(2)	136.5(2)
O(1)−Zn(1)−N(3)	135.1(2)	N(1)−Zn(1)−N(2)	80.6(2)
N(1)−Zn(1)−N(3)	80.3(2)	N(1)−Zn(1)−O(2)	172.7(2)
N(2)−Zn(1)−N(3)	85.0(2)	N(2)−Zn(1)−O(2)	93.4(2)
N(3)−Zn(1)−O(2)	103.4		

[a] Estimated standard deviations indicated in parentheses.

Resonance Raman spectra of frozen solutions of $[L^{tBu_2}Cu(CH_3CN)]O_3SCF_3$ and $L^{tBu_4}Cu$ in CD_3CN obtained by excitation into the LMCT bands are shown in Figure 5a,b. They contain high-frequency features typical of metal−phenolate complexes. For example, metal−tyrosinate proteins give rise to characteristic vibrations at *ca.* 1170, 1270, 1500, and 1600 cm^{-1} that derive mainly from ring deformations ν_{9a}, ν_{7a}, ν_{19a}, and ν_{9a}, respectively.[28,29] Corresponding peaks are found at similar energies in the spectra shown in Figure 5a,b, but the increased substitu-

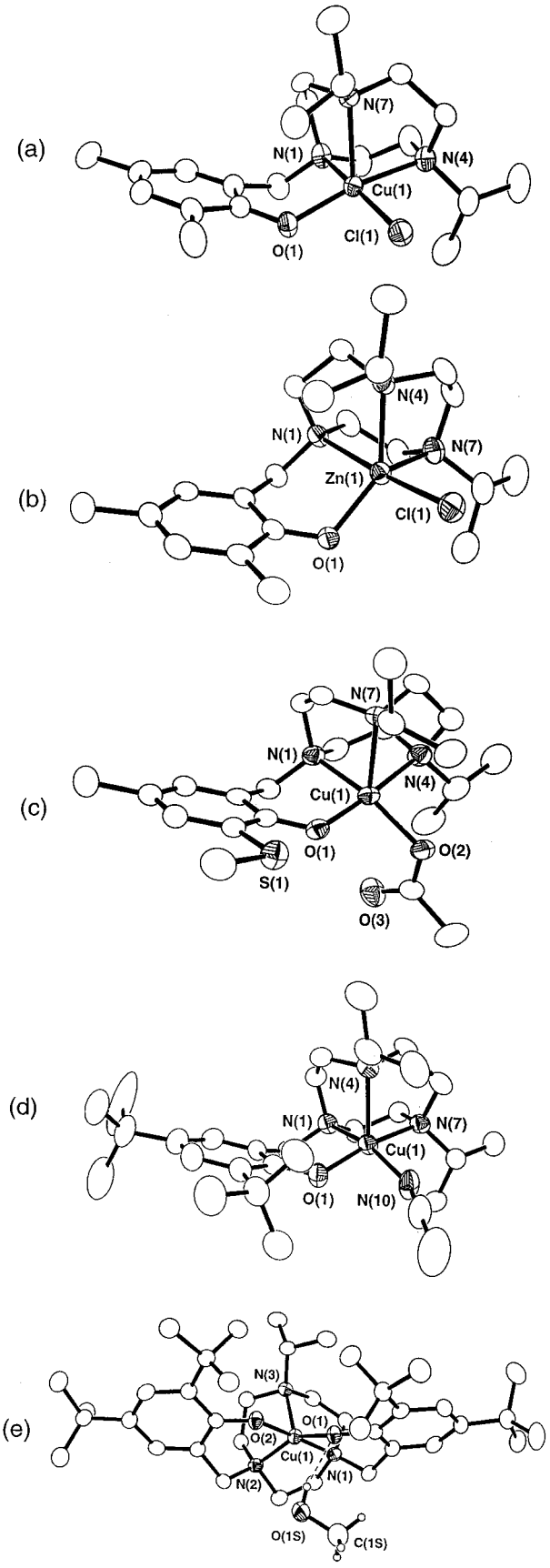

Figure 3. Drawings of the X-ray crystal structures of (a) $L^{Me_2}CuCl$, (b) $L^{Me_2}ZnCl$, (c) $L^{MeSMe}Cu(O_2CCH_3)$, (d) the cationic fragment of $[L^{tBu_2}Cu(CH_3CN)]O_3SCF_3\cdot C_7H_8$, and (e) $L^{tBu_4}Cu\cdot MeOH$. With the exception of structure e, which shows the MeOH solvate molecule involved in hydrogen bonding to the copper complex, solvate molecules and hydrogen atoms are omitted for clarity. All ellipsoids are drawn at the 50% probability level.

(28) Que, L., Jr. In *Biological Applications of Raman Spectroscopy;* Spiro, T. G., Ed.; John Wiley & Sons: New York, 1988; Vol. 3, pp 491−521. (b) Que, L., Jr. *Coord. Chem. Rev.* **1983**, *50,* 73.

(29) (a) Mukherjee, A.; McGlashen, M. L.; Spiro, T. G. *J. Phys. Chem.* **1995**, *99,* 4912−4917. (b) McGlashen, M. L.; Eads, D. D.; Spiro, T. G.; Whittaker, J. W. *J. Phys. Chem.* **1995**, *99,* 4918−4922.

Table 3. UV−Vis Absorption Spectral Data for Cu^{II}−Phenolate and M^{II}−Phenoxyl Radical Species (M = Cu or Zn)

complex	λ_{max}, nm (ϵ, M^{-1} cm^{-1})[a]		
	Cu^{II}−Phenolates		
$L^{Me_2}CuCl$	340 (3100)	520 (1500)	710 (sh, 440)
$L^{tBu_2}CuCl$	350 (3000)	526 (1200)	720 (sh, 400)
$L^{MeOMe}CuCl$		528 (1150)[b]	
$L^{tBuSMe}CuCl$		530 (950)[b]	
$L^{tBu_2}Cu(O_2CCH_3)$		474 (960)[b]	
$L^{MeOMe}Cu(O_2CCH_3)$		486 (900)[b]	
$L^{MeSMe}Cu(O_2CCH_3)$		484 (810)[b]	
$[L^{tBu_2}Cu(CH_3CN)]CF_3SO_3$	342 (3600)	538 (1440)	660 (sh, 700)[c]
$L^{tBu_4}Cu$·MeOH	300 (18000)	448 (1800)	706 (430)[d]
inactive GAO		438 (1000)	625 (1167)[e,f]
inactive GAO azide	375 (1880)	559 (642)	747 (500)[e,f]
inactive GLO		451 (1875)	678 (1365)[e]
inactive GLO azide	370 (2670)	564 (1248)	728 (888)[e]
	Cu^{II}− and Zn^{II}−Phenoxyl Radicals		
$[L^{tBu_2}Cu(CH_3CN)]^{2+}$	410 (4000)	422 (sh, 3800)	672 (1000)[g]
$[L^{tBu}ZnCl]^{2+}$	396 (2600)	406 (2650)	690 (250)[d]
$[L^{tBu_4}Cu]^{+}$	398 (3900)	568 (2200)	646 (2200)[h]
$[L^{tBu_4}Zn]^{+}$	394 (sh, 2900)	408 (3200)	722 (400)[d]
active GAO		444 (5194)	800 (3211)[e,f]
active GLO		448 (5700)	851 (4300)[e]

[a] Except where noted, spectra measured on CH_2Cl_2 solutions at room temperature. [b] Additional intensity is present at longer wavelengths (~600−800 nm), but no bands are clearly resolved. [c] 10:1 CH_2Cl_2/CH_3CN. [d] CH_2Cl_2, −40 °C. [e] Reference 2. [f] Whittaker, M. M.; Whittaker, J. W. *J. Biol. Chem.* **1988**, *263*, 6074−6080. [g] ~5:1 CH_2Cl_2/CH_3CN, −40 °C. [h] 1:0.1 CH_2Cl_2/CH_3CN, −40 °C.

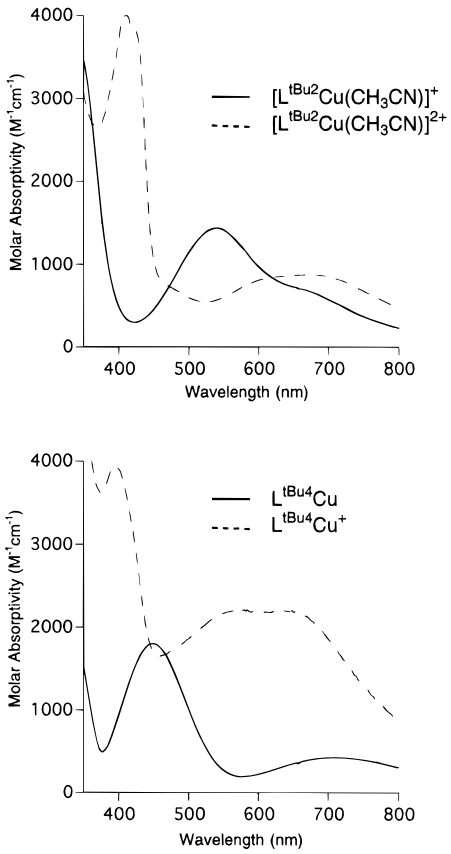

Figure 4. Optical absorption spectra of (top) $[L^{tBu_2}Cu(CH_3CN)]O_3SCF_3$ in CH_2Cl_2 (—) and $[L^{tBu_2}Cu(CH_3CN)]^{2+}$ resulting from oxidation by 1 equiv of Ce^{IV} in 5:1 CH_2Cl_2/CH_3CN at −40 °C (- - -) and (bottom) $L^{tBu_4}Cu$ in CH_2Cl_2 (—) and $[L^{tBu_4}Cu]^{+}$ resulting from oxidation by 1 equiv of Ce^{IV} in 1:0.1 CH_2Cl_2/CH_3CN at −40 °C (- - -).

tion of the phenolates in L^{tBu_2} and L^{tBu_4} relative to the tyrosinate moiety very likely gives rise to the multiplicity of some of the features.[13a] The ν_{7a} and ν_{8a} modes for the axial, non-redox-active tyrosinate ligand in the inactive form of glyoxal oxidase (pH 8.1) occur at 1260 and 1609 cm^{-1} and for the cysteine-modified tyrosinate at 1267 and 1596 cm^{-1}, respectively, close to their positions in the model compound spectra.[2]

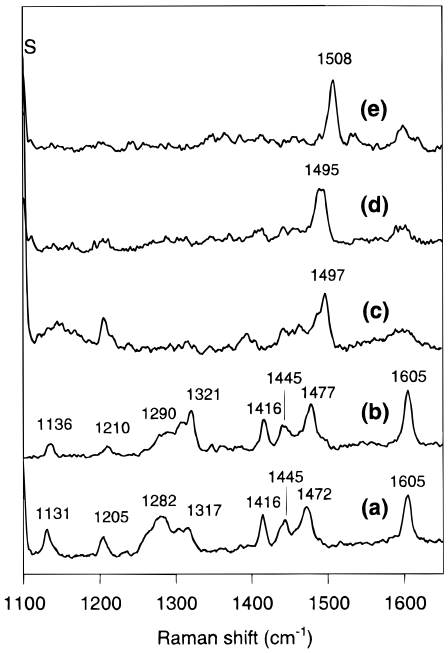

Figure 5. Resonance Raman spectra of (a) $[L^{tBu_2}Cu(CH_3CN)]^{+}$, (b) $L^{tBu_4}Cu$, (c) $[L^{tBu_2}Cu(CH_3CN)]^{2+}$, (d) $[L^{tBu_4}Cu]^{+}$, and (e) $[L^{tBu_4}Zn]^{+}$. All spectra were acquired on frozen solutions at −196 °C in CD_2Cl_2 [spectrum b] or CD_2Cl_2/CD_3CN mixtures [spectra a and c−e], with excitation wavelengths of 514.5 nm [spectrum a] or 457.9 nm [spectra b−e].

Table 4. Electrochemical Data from Cyclic Voltammetry Experiments[a]

complex	$E_{1/2}$ (V)[b]	ΔE_p (mV)	complex	$E_{1/2}$ (V)[b]	ΔE_p (mV)
$L^{tBu_2}CuCl$	0.56	86	$L^{tBu_4}Cu$	0.50	93
$L^{tBu_2}ZnCl$	0.52	69		0.78	99
$L^{tBuSMe}CuCl$	0.51	82	$L^{tBu_4}Zn$	0.48	83
$L^{tBuSMe}ZnCl$	0.49	70		0.81	85
$[L^{tBu_2}Cu(CH_3CN)]^{+}$	0.79	92			

[a] All experiments were performed using CH_2Cl_2 with 0.4 M tetrabutylammonium hexafluorophosphate ($TBAPF_6$), scan rate 100 mV s^{-1}, room temperature, $i_{pa} \approx i_{pc}$. [b] Reported versus SCE.

B. Cu^{II}− and Zn^{II}−Phenoxyl Radical Complexes. Electrochemistry. Without exception, the $L^{RR'}CuX$ (X = Cl, O_2CCH_3) complexes and their Zn^{II} analogs supported by the ligands L^{Me_2}, L^{MeOMe}, and L^{MeSMe} exhibit irreversible oxidation processes in their cyclic voltammograms (0.4 M $TBAPF_6$ in CH_2Cl_2 or CH_3CN). We attribute this behavior to decomposition of the electrochemically generated species via C−C bond coupling processes involving the benzylic positions *para* to the phenolate (phenoxyl) oxygen atom, where significant spin density in phenoxyl radicals is known to reside and to contribute to enhanced reactivity.[30]

In contrast, the cyclic voltammograms (CH_2Cl_2, 0.4 M $TBAPF_6$) of complexes with *tert*-butyl groups in the positions *para* to the phenolate oxygen atoms are characterized by electrochemically (ΔE_p < 100 mV) and chemically ($i_{pc} \approx i_{pa}$) reversible redox processes (Table 4). Controlled potential coulometric experiments with the monophenolate compounds revealed that these redox processes correspond to the transfer of one electron. For example, low-temperature (−40 °C) electrolysis of a solution of $[L^{tBu_2}Cu(CH_3CN)]^{+}$ in CH_2Cl_2 (0.4

(30) (a) Rigby, S. E. J.; Nugent, J. H. A. *Biochemistry* **1994**, *33*, 1734−1742. (b) O'Malley, P. J.; MacFarlane, A. J.; Rigby, S. E. J.; Nugent, J. H. A. *Biochim. Biophys. Acta* **1995**, *1232*, 175−179.

M $TBAPF_6$) at 1.0 V vs SCE resulted in the removal of 0.8 ± 0.1 e^- mol^{-1} of complex and a color change from purple to deep green; similar color changes were observed upon coulometric oxidation of $L^{tBu_2}CuCl$ (purple to deep green) and L^{tBu_2}-ZnCl (colorless to light green). UV−vis spectroscopic (at −40 °C) analysis of the EPR-silent (at 77 K, X-band) green solution obtained after the electrochemical oxidation of $[L^{tBu_2}Cu(CH_3CN)]^+$ revealed the presence of new optical absorption features with $\lambda_{max} = 410$ ($\epsilon = 3500$ M^{-1} cm^{-1}) and 648 (1000) nm. On the basis of the resemblance of the 410 nm feature to similar bands in activated GAO and GLO (Table 3) and hindered phenoxyl radicals,[31] as well as other chemical and spectroscopic evidence (*vida infra*), we postulate that one-electron oxidation results in the generation of a Cu^{II}−phenoxyl radical complex. The assignment of the oxidation process as ligand-based and not as a Cu^{II}/Cu^{III} couple is supported by the observation of similar redox behavior for the Zn^{II}−phenolate compounds (albeit at a slightly different potential), in which the central metal ion is not redox active.

The lower redox potential of $L^{tBu_2}CuCl$ (0.56 V) compared to the related complex $[L^{tBu_2}Cu(CH_3CN)]^+$ (0.79 V) may be attributed to the increased electron-donating ability of the chloride ligand compared to the acetonitrile donor. More interestingly, comparison of the electrochemical data for L^{tBuSMe}-MCl (M = Cu or Zn) with the data obtained for the analogous complexes $L^{tBu_2}MCl$ (Table 4) reveals a modest lowering of the $E_{1/2}$ values in the thioether-appended systems (by 50 mV for Cu and 30 mV for Zn). Thus, the electron-releasing property of the *o*-SMe group (indicated, for example, by the lower energy of the LMCT band in the Cu^{II} complex of L^{tBuSMe} compared to that of L^{tBu_2}; Table 3) facilitates formation of the metal−phenoxyl radical complexes by lowering the phenolate/phenoxyl radical redox potential, albeit not by a large amount. These spectroscopic and electrochemical observations support the notion that the *o*-cysteine modification of the redox active tyrosinate ligand in the active sites of GAO and GLO serves in part to facilitate the oxidation of the Cu^{II}−Y272 pair to Cu^{II}−Y272$^\bullet$ by O_2 during the last step in the proposed enzyme mechanism(s),[1,4] although the effect appears to be moderate on the basis of our observations with the synthetic compounds. Other structural and/or electronic influences that are present in the protein but are absent in the model complexes (e.g., the π-stacking interaction with the nearby tryptophan residue) also would be expected to contribute in nontrivial ways to the control of the Y272/Y272$^\bullet$ redox potential, which at $E_{1/2} = 0.23$ V vs SCE is significantly lower than those we have observed.[32]

The cyclic voltammograms of the diphenolate complexes $L^{tBu_4}M$ (M = Cu or Zn) contain two reversible, one-electron waves (Figure 6, Table 4). Again, the close correspondence of the data for the Cu^{II} and Zn^{II} compounds of L^{tBu_4} argues for a ligand- rather than a metal-centered process to yield a M^{II}−phenoxyl radical species in the first oxidation; this is further supported by spectroscopic data *(vide infra).* Note that simultaneous phenolate and phenoxyl radical coordination is implicated for these systems, just as in the active forms of GAO and GLO. The second reversible oxidation also occurs at similar potentials for the copper and zinc compounds, suggesting that it involves another ligand-centered oxidation to M^{II}−$(phenoxyl)_2$ species, $[L^{tBu_4}M]^{2+}$. Experiments aimed at confirming this formulation and unraveling the magnetochemical properties of these compounds are underway and will be reported separately.

Chemical Synthesis and Spectroscopic Properties. In addition to being accessible via electrochemical methods, we were able to generate M^{II}−phenoxyl radical species that are

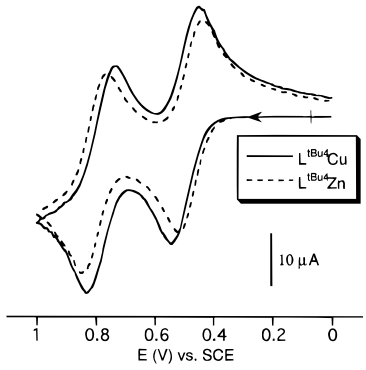

Figure 6. Cyclic voltammograms of $L^{tBu_4}M$ (M = Cu or Zn) in CH_2Cl_2 (0.4 M $TBAPF_6$).

Scheme 4

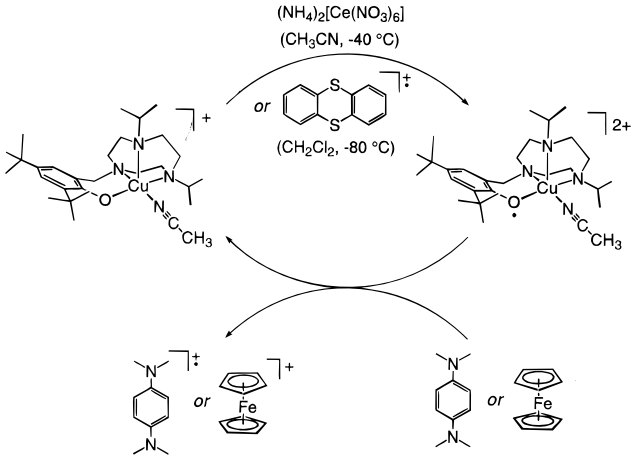

stable in solution at low temperature[33] by using either of the two one-electron oxidants $(NH_4)_2[Ce(NO_3)_6]$ or [thianthryl]-BF_4,[13a,34] both of which have the added advantage of existing as spectroscopically (EPR, UV−vis, resonance Raman) innocent species in their reduced forms $[Ce(NO_3)_3$ and thianthrene, respectively]. For example, treatment of CH_2Cl_2 solutions of $[L^{tBu_2}Cu(CH_3CN)]^+$ with stoichiometric amounts of either $(NH_4)_2[Ce(NO_3)_6]$ in CH_3CN at −40 °C or [thianthryl]BF_4 in CH_2Cl_2 at −80 °C resulted in a color change from purple to deep green (Scheme 4). These green solutions are EPR silent (X-band, 92 ± 5% by double integration of the residual signal at 77 K), consistent with magnetic coupling between an $S = 1/2$ Cu^{II} ion and an $S = 1/2$ phenoxyl radical. The type of coupling is unclear at present; antiferromagnetic coupling between a coordinated phenoxyl radical and a central metal ion was observed by Wieghardt and co-workers in a Fe^{III}−phenoxyl radical complex ($J = -88$ cm^{-1})[13a,c] and a structurally characterized Cr^{III}−phenoxyl radical compound,[13b] but ferromagnetic interactions ($S = 1$ ground state) have been identified in equatorial coordinated Cu^{II}−semiquinato complexes that are EPR silent at X-band frequency due to large zero field splitting.[35] Extensive magnetochemical studies to address this issue are planned. The UV−vis spectrum of the green product (Figure 4) is similar to that of the electrochemically oxidized solution, the feature at ∼415 nm ($\epsilon \approx 3900$ M^{-1} cm^{-1}) similar to that reported for the active forms of GAO and GLO[1,2] being indicative of a coordinated phenoxyl radical. Both EPR and

(31) Altwicker, E. R. *Chem. Rev.* **1967**, *67*, 475−531.
(32) Dyrkacz, G. R.; Libby, R. D.; Hamilton, G. A. *J. Am. Chem. Soc.* **1976**, *98*, 626−628.
(33) Repeated attempts to isolate the oxidized products as pure solids have yet to be successful.
(34) Boduszek, B.; Shine, H. J. *J. Org. Chem.* **1988**, *53*, 5142−5143.
(35) For example, see: (a) Kahn, O.; Prins, R.; Reedijk, J.; Thompson, J. S. *Inorg. Chem.* **1987**, *26*, 3557−3561. (b) Benelli, C.; Dei, A.; Gatteschi, D.; Pardi, L. *Inorg. Chem.* **1990**, *29*, 3409−3415. (c) Dei, A.; Gatteschi, D.; Pardi, L.; Barra, A. L.; Brunel, L. C. *Chem. Phys. Lett.* **1990**, *175*, 589−592.

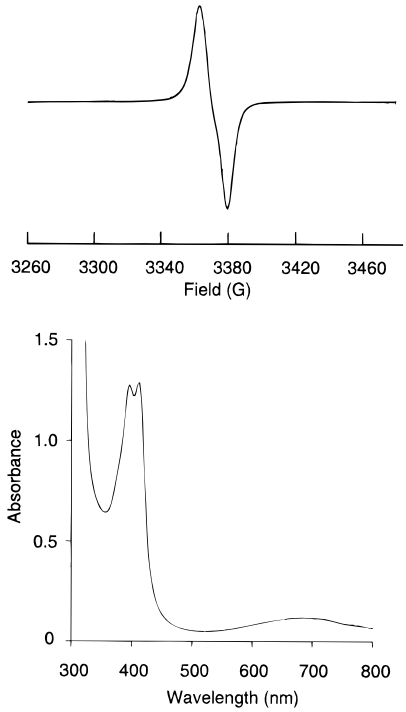

Figure 7. X-band EPR (top, 1:1 CH_2Cl_2/toluene, −196 °C) and UV−vis (bottom, CH_2Cl_2, 0.49 mM, −40 °C) spectra of $[L^{tBu_2}ZnCl]^+$.

UV−vis titrations established the 1:1 stoichiometry of the oxidation reaction, confirming the previously discussed coulometric results.

Similar one-electron oxidations of $L^{tBu_2}ZnCl$ and $L^{tBu_4}M$ (M = Cu or Zn) were performed; the spectroscopic data for the resulting M^{II}−phenoxyl radical species are listed in Table 3 and shown for $[L^{tBu_2}ZnCl]^+$ in Figure 7. The optical absorption data are fairly similar for all of the compounds, although the intensity of the longer wavelength features is greater for the Cu^{II} complexes than for the Zn^{II} cases, consistent with the expected magnitude of additional contributions from ligand field transitions in this region for the different ions. Moreover, the monoradical derived from $L^{tBu_4}Cu$ exhibits greater intensity in the 500−700 nm region than shown by those prepared from the $L^{tBu_2}Cu^{II}$ complexes (Figure 4), presumably due to the presence of mixed phenolato−phenoxyl radical ligation. We speculate that a low-energy $PhO^- \rightarrow Cu^{II}$ LMCT (significantly shifted to longer wavelength than in the reduced precursor L^{tBu_4}-Cu, which has higher energy metal-based acceptor orbitals) and a ligand field transition(s) are major contributors to this absorption intensity in the monoradical.[36] Additional intensity increases in this region, as well as new features, appear upon further oxidation of $[L^{tBu_4}M]^+$ (M = Cu or Zn) with Ce^{IV} (data not shown). These observations are consistent with the electrochemical results described above that suggest that a unique $M^{II}-(phenoxyl)_2$ species is generated upon two-electron oxidation of $L^{tBu_4}M$ (under investigation). The UV−vis data for the Zn^{II}−phenoxyl radical compounds (cf. Figure 7) are similar to those reported for $[Zn(BIDPhE)Cl_2]$,[11,12] which contains a pendant, noncoordinated 2,4,6-trisubstituted phenoxyl radical and has absorption maxima at 378 nm (ϵ = 1500 M^{-1} cm^{-1}), 394 nm (1700), and 638 nm (430). These features are shifted to higher energy than those for the L^{tBu_2} and L^{tBu_4} compounds, however. The lower energy of the bands for the compounds we have prepared appears to be a consequence of coordination of the phenoxyl radical to the metal ion. Finally, while both Cu^{II}−phenoxyl radical compounds do not give rise to an EPR signal, the Zn^{II} complexes exhibit nearly isotropic signals (∼19 G width, peak-to-trough) centered at g = 2.00 in their X-band EPR spectra at 77 K (Figure 7). Double integration of these signals revealed the appropriate intensity for their formulations as monooxidized Zn^{II}−phenoxyl radicals.

Consistent with the reversible behavior apparent in cyclic voltammograms of the M^{II}− phenolate precursors, reduction of the chemically synthesized M^{II}−phenoxyl radical complexes could be effected electrochemically or via stoichiometric reaction with ferrocene (Fc) or *N*,*N*,*N*′,*N*′-tetramethyl-1,4-phenylenediamine (TMPDA; cf. Scheme 4). For example, the cyclic voltammograms (initial scan cathodic) of the oxidized complexes $[L^{tBu_2}ZnCl]^{2+}$ and $[L^{tBu_4}Cu]^+$ (CH_2Cl_2, 0.4 M $TBAPF_6$, −40 °C) are the exact complements of those of their respective starting materials (initial scan anodic). Also, treatment of the green solution of $[L^{tBu_2}Cu(CH_3CN)]^{2+}$ in CH_2Cl_2 at −40 °C with Fc or TMPDA as monitored by UV−vis spectroscopy revealed quenching of the Cu^{II}−phenoxyl radical features and growth of those of the Cu^{II}−phenolate complex and either Fc^+ (λ_{max} = 620 nm) or the TMPDA radical cation (λ_{max} = 570 nm, ϵ = 12500 M^{-1} cm^{-1}).[37] Titrations established a 1:1 stoichiometry for these reactions.

Further evidence in support of the formulation of the M^{II}−phenoxyl radical compounds was obtained from resonance Raman spectroscopy of the solutions resulting from one-electron oxidation of $[L^{tBu_2}Cu(CH_3CN)]^+$ and $L^{tBu_4}Cu$ (Figure 5). The phenolate vibrations of the precursor complexes (Figure 5a,b) are replaced by one prominent feature at 1495−1497 cm^{-1} upon oxidation (Figures 5c,d). This peak also is observed at 1508 cm^{-1} in $[L^{tBu_4}Zn]^+$ (Figure 5e) and is assigned to ν_{7a} of the phenoxyl radical ligand by analogy to similar features in other species that contain such a radical, e.g., activated GAO (1487 cm^{-1}),[29b] the R2 protein of ribonucleotide reductase (1498 cm^{-1}),[38] and a diiron(III) model complex (1504 cm^{-1}).[11,12] The ν_{7a} vibration has a significant C−O bond stretching component, and its shift to higher energy relative to that of the precursor complex is consistent with the increased double bond character expected for the oxidized species.[29,39] In addition, there are weaker features at *ca*. 1200 and near 1400 cm^{-1} that resemble the positions and relative intensities of vibrations found in the active forms of GAO and GLO which are attributed to the coordinated tyrosyl radical.[2,29b]

Conclusions

By using new ligands comprised of one or two phenolate donors appended to the strongly binding 1,4,7-triazacyclononane frame, we have prepared and characterized a series of Cu^{II} complexes that model the inactive forms of GAO and GLO. The effect of the cysteine modification of the equatorial tyrosinate ligand in the proteins was probed through the study of isostructural series of complexes of ligands having varying appendages, including biomimetic *o*-thioethers, on the phenolate ligand. The alkylthio group was found to induce relatively small shifts of the $PhO^- \rightarrow Cu^{II}$ LMCT band and the Cu^{II}−phenolate/Cu^{II}−phenoxyl radical redox potential consistent with increased electron density on the ring relative to alkyl-substituted reference

(36) A Cu^{II}−mediated phenolate-to-phenoxyl radical CT transition may also be considered as contributing to the added intensity, although this type of process ascribed to the proteins occurs at significantly longer wavelength (λ_{max} = 800 nm).[29b] We anticipate that the disposition of the phenolate and phenoxyl ligands would affect the energy and intensity of such a CT, however, and based on the crystallographic data for the $L^{tBu_4}M$ complexes that show a difference between the relative geometries of these ligands compared to the proteins a corresponding divergence in the CT bands would not be surprising.

(37) Fujita, S.; Steenken, S. J. *Am. Chem. Soc.* **1981**, *103*, 2540−2545.
(38) Bender, C; Sahlin, M; Babcock, G. T.; Chandrashekov, T. L.; Sabowe, S. P.; Stubbe, J.; Lindstrom, B.; Petersson, L.; Ehrenberg, A.; Sjoberg, B.-M. *J. Am. Chem. Soc.* **1989**, *111*, 8076−8083.
(39) Tripathi, G. N. R.; Schuler, R. H. *J. Phys. Chem.* **1988**, *92*, 5129−5133.

systems. The presence of the cysteine modification in the proteins thus may be rationalized, at least in part, by invoking analogous electronic influences that help to stabilize the Cu^{II}−tyrosyl radical state. Low-temperature electrochemical and chemical oxidation of the Cu^{II} and Zn^{II} complexes having *tert*-butyl protecting groups on the phenolate ligands yielded novel M^{II}−phenoxyl radical compounds akin to the active forms of GAO and GLO. Identification of the oxidation as ligand-rather than metal-centered is based on (i) the nearly identical electrochemical behavior of similar Cu^{II} and Zn^{II} complexes and (ii) the observation of UV−vis and resonance Raman signatures of the phenoxyl radical, with additional corroboration from EPR and UV−vis data for the paramagnetic Zn^{II} cases. Although stable for hours at temperatures below −40 °C, the metal−phenoxyl radical complexes rapidly decompose to unidentified products at room temperature, presumably via radical disproportionation. This behavior stands in sharp contrast to the tri- and tetravalent metal complexes of bis(phenolate)mono(phenoxyl radical) ligands reported by Wieghardt to be stable at room temperature.[13] We speculate that facile dissociation (or solvent- or counterion-assisted displacement) of the lower denticity phenoxyl radical ligand from the Cu^{II} or Zn^{II} centers that have an additional, potentially labile monodentate ligand yields a "free" radical that is prone to decompose.[40]

Although progress toward understanding the nature of the unusual GAO and GLO active sites has been attained through the characterization of the Cu^{II}−phenoxyl radical complexes we have prepared, shortcomings of the complexes as structural, spectroscopic, and functional models need to be addressed. For example, the intense, low-energy optical absorption ($\lambda_{max} = 800$ nm, ϵ 3200 M^{-1} cm^{-1}) attributed to charge transfer between the axial tyrosinate and the equatorial tyrosyl radical in active GAO and GLO has yet to be seen in a synthetic compound, necessitating deeper exploration of the oxidation chemistry of complexes with multiple phenolate donors. Oxidation of a mixed Cu^{II}−alcoholato/phenolato complex had been shown previously to yield aldehyde in a reaction modeling GAO function,[15] and in a recent report treatment of an exogenous alcohol with a preformed Cu^{II}−phenoxyl radical to generate aldehyde in a model "single-turnover" reaction was reported.[14a,41] Mechanistic understanding of the reactions is lacking, however. Current research continues to be inspired by these and other issues that are pertinent not only to GAO and GLO structure and function, but also within a broader context to the fundamental chemistry of metal−radical arrays in biological systems.[8]

Experimental Section

General Procedures. All reagents and solvents were obtained from commercial sources and used as received unless otherwise noted. Solvents were dried according to published procedures and distilled under N_2 immediately prior to use. Commercial NaH (60% dispersion in oil) was washed with pentane to remove the dispersant, dried under vacuum, and stored under a dry, inert atmosphere. All transition metal complexes were synthesized in a Vacuum Atmospheres inert atmosphere glovebox under a dry N_2 atmosphere. Spectroscopic and analytical data were collected as described previously.[17b] Quantitation of EPR signal intensity was accomplished by comparison to standard solutions of $[L^{iPr_3}Cu(O_3SCF_3)(H_2O)]CF_3SO_3$[25] in 1:1 CH_2Cl_2/toluene or $CuSO_4$ in glycerol/H_2O (for copper complexes) or 2,2,6,6-tetramethyl-1-piperidinyloxy (TEMPO) in toluene (for the zinc−phenoxyl radical complexes).

4-Methyl-2-(methylthio)phenol.[21] A 100 mL Schlenk flask fitted with a gas adaptor and a pressure equalizing addition funnel was charged with 6.60 g of $KMnO_4$; this apparatus was connected via a Teflon cannula to another 100 mL Schlenk flask which was charged with H_2SO_4 (22 mL). The flask containing the H_2SO_4 was cooled to 0 °C, and dimethyl sulfide (DMS; 7.0 g, 113 mmol) was added via syringe. After the entire apparatus was purged with N_2 for 30 min, HCl (40 mL) was placed in the dropping funnel, and the tip of the Teflon cannula connecting the two halves of the reaction apparatus placed below the surface of the H_2SO_4/DMS solution. The HCl was then added dropwise to the solid $KMnO_4$ with vigorous stirring, causing the evolution of Cl_2 (g), which was swept into the H_2SO_4/DMS mixture with a gentle N_2 flow. The addition of HCl took place over 45 min, and the H_2SO_4/DMS mixture was maintained at 0 °C. Subsequently, 4-methylphenol (5.0 g, 46.2 mmol) was added to the chlorodimethylsulfonium bisulfate mixture via syringe over a period of 1 h, causing the evolution of HCl(g). After the addition of 4-methylphenol, the mixture was removed from the ice bath and was stirred at room temperature for 1 h. The yellow mixture was then poured into a solution of NaCl (25 g) in H_2O (160 mL), and the resultant solution heated at reflux overnight. After the reflux period, the heterogenous mixture was cooled to room temperature and the insoluble oil removed by extraction with Et_2O (150 mL). The Et_2O phase was dried (Na_2SO_4) and the solvent evaporated under reduced pressure to yield a yellow oil. Vacuum distillation (bp 55−65 °C, 0.05 Torr) of the crude product yielded a colorless oil, 2.45 g (34% based on 4-methylphenol): ^{1}H NMR (300 MHz, $CDCl_3$) δ 7.27 (d, J = 1.5 Hz, 1H), 7.03 (dd, J = 2.1, 8.4 Hz, lH), 6.86 (d, J = 8.4 Hz, 1H), 6.45 (s, 1H), 2.30 (s, 3H), 2.25 (s, 3H) ppm; LREIMS *m/z* 154 [M^+].

4-*tert*-Butyl-2-(methylthio)phenol. This compound was prepared in a fashion similar to that described above for 4-methyl-2-(methylthio)-phenol, substituting 4-*tert*-butylphenol. Vacuum distillation afforded the pure product as a colorless oil (bp 88−90 °C, 0.05 Torr): ^{1}H NMR (300 MHz, $CDCl_3$) δ 7.50 (d, J = 2.1 Hz, 1H), 7.29 (dd, J = 2.1, 8.7 Hz, 1H), 6.93 (d, J = 8.7 Hz, 1H), 6.51 (s, 1H), 2.34 (s, 3H), 1.30 (s, 9H) ppm; LREIMS *m/z* 196 [M^+].

Synthesis of Ligands $HL^{RR'}$. The following procedure for the preparation of 1-(2-hydroxy-3,5-dimethylbenzyl)-4,7-diisopropyl-1,4,7-triazacyclononane (HL^{Me_2}) is typical for the class, with the only variation for the different examples being the phenol used in the condensation reaction (Scheme 1). To a solution of 1,4-diisopropyl-1,4,7-triazacyclononane[17] (1.057 g, 4.95 mmol) in MeOH (15 mL) was added aqueous formaldehyde (0.538 g, 6.64 mmol), and the resultant solution heated at reflux for 1.5 h. A solution of 2,4-dimethylphenol (0.630 g, 5.16 mmol) in MeOH (5 mL) was added, and refluxing was continued overnight. After cooling to room temperature, H_2O (5 mL) was added to the yellow solution, causing the deposition of a colorless oil. This oil was collected by carefully decanting away the supernatant, and subsequently redissolved in Et_2O (20 mL) and washed with 3 M NaOH. The Et_2O phase was removed and dried with Na_2SO_4; evaporation of the solvent under reduced pressure yielded the product as a colorless oil which crystallized on standing (1.224 g, 71%): ^{1}H NMR (500 MHz, $CDCl_3$) δ 6.81 (s, 1H), 6.60 (s, 1H), 3.73 (s, 2H), 2.98 (br m, 4H), 2.88 (heptet, J = 6.5 Hz, 2H), 2.67 (t, J = 4.5 Hz, 4H), 2.43 (s, 4H), 2.19 (s, 3H), 2.17 (s, 3H), 0.95 (d, J = 6.5 Hz, 12H) ppm; HREIMS calcd for $C_{21}H_{37}N_3O$ 347.2936, found 347.2936. Anal. Calcd for $C_{2l}H_{37}N_3O$: C, 72.58; H, 10.73; N, 12.09. Found: C, 71.95; H, 10.52; N, 11.97.

1-(3,5-Di-*tert*-butyl-2-hydroxybenzyl)-4,7-diisopropyl-1,4,7-triazacyclononane (HL^{tBu_2}): Yield 90%; ^{1}H NMR (300 MHz, $CDCl_3$) δ 7.17 (d, J = 2.4 Hz, 1H), 6.81 (d, J = 2.4 Hz, 1H), 3.76 (s, 2H), 3.04−2.85 (overlapping m and heptet (J = 6.6 Hz), 6H), 2.68 (t, J = 4.8 Hz, 4H), 2.46 (s, 4H), 1.42 (s, 9H), 1.28 (s, 9H), 0.97 (d, J = 6.6 Hz, 12H) ppm; LREIMS *m/z* 431 [M^+]. Anal. Calcd for $C_{27}H_{49}N_30$: C, 75.12; H, 11.44; N, 9.73. Found: C, 74.61; H, 11.22; N, 9.24.

1-(2-Hydroxy-3-methoxy-5-methylbenzyl)-4,7-diisopropyl-1,4,7-triazacyclononane (HL^{MeOMe}): yield 63%; ^{1}H NMR (300 MHz, $CDCl_3$) δ 8.99 (br, 1H), 6.57 (s, 1H), 6.37 (s, 1H), 3.82 (s, 3H), 3.76 (s, 2H), 3.01 (m, 4H), 2.88 (heptet, J = 6.6 Hz, 2H), 2.69 (t, J = 4.8 Hz, 4H), 2.43 (s, 4H), 2.22 (s, 3H), 0.94 (d, J = 6.6 Hz, 12H) ppm; HREIMS calcd for $C_{21}H_{37}N_3O_2$ 363.2886, found 363.2888. Anal. Calcd for $C_{21}H_{37}N_3O_2$: C, 69.38; H, 10.26; N, 11.56. Found: C, 68.75; H, 10.22; N, 11.44.

(40) Presumably, this decomposition is facilitated by the presence of unpaired spin density at the unprotected benzylic position (where the phenolate is linked to the macrocycle). The design and synthesis of new ligands protected at this position is underway (Jazdzewski, B. A., Tolman, W. B. Unpublished results).

(41) We have explored the stoichiometic reactions of the Cu^{II}−phenoxyl radical complexes described herein with alcohols, but have yet to observe significant yields of aldehydes.

1-(2-Hydroxy-5-methyl-3-(methylthio)benzyl)-4,7-diisopropyl-1,4,7-triazacyclononane (HL^{MeSMe}): yield 70%; ^{1}HNMR (300 MHz, $CDCl_3$) δ 11.16 (br, 1H), 6.86 (d, J = 1.8 Hz, 1H), 6.58 (d, J = 1.8 Hz, 1H), 3.74 (s, 2H), 3.02 (br m, 4H), 2.89 (heptet, J = 6.6 Hz, 2H), 2.67 (t, J = 4.8 Hz, 4H), 2.42 (s, 4H), 2.41 (s, 3H), 2.22 (s, 3H), 0.94 (d, J = 6.6 Hz, 12H) ppm. Anal. Calcd for $C_{21}H_{37}N_3OS$: C, 66.45; H, 9.82; N, 11.07; S, 8.45. Found: C, 66.26; H, 9.81; N, 11.15; S, 8.54.

1-(4-*tert*-Butyl-2-hydroxy-3-(methylthio)benzyl)-4,7-diisopropyl-1,4,7-triazacyclononane (HL^{tBuSMe}): yield 55%; ^{1}H NMR (500 MHz, CDC1$_3$) δ 7.11 (d, J = 2.0 Hz, 1H), 6.78 (d, J = 2.0 Hz, 1H), 3.78 (s, 2H), 3.03 (br m, 4H), 2.90 (heptet, J = 6.5 Hz, 2H), 2.68 (t, J = 4.8 Hz, 4H), 2.43 (br s, 7H), 1.26 (s, 9H), 0.95 (d, J = 6.5 Hz, 12H) ppm. Anal. Calcd for $C_{24}H_{43}N_3OS$: C, 68.36; H, 10.28; N, 9.96. Found: C, 67.79; H,10.00; N, 9.74.

1-Isopropyl-1,4,7-triazacyclononane. To a solution of 1,4-ditosyl-1,4,7 triazacyclononane[22] (11.99 g, 0.027 mol) in distilled CH_3CN (120 rnL) was added 2-bromopropane (7.40 g, 0.060 mol), Na_2CO_3 (6.49 g, 0.060 mol), and tetrabutylammonium bromide (20 mg). The resulting solution was heated at reflux under N_2 for 36 h. The reaction mixture was then cooled to ambient temperature and filtered, and the remaining solids were washed with CH_2Cl_2 (100 mL). The combined organic filtrates were dried over $MgSO_4$. Following filtration, the solvents were removed under reduced pressure, yielding a thick, pale yellow oil. The isolated oil was then dissolved in 18 M H_2SO_4 (60 mL), and the resulting dark brown solution was heated at 120 °C under N_2 for 40 h. After cooling to room temperature, the dark mixture was poured into crushed ice (100 g), and aqueous NaOH was added until the pH of the solution exceeded 11. The brown solution was then extracted with $CHCl_3$ (4 × 300 mL). The combined $CHCl_3$ fractions were dried ($MgSO_4$), and the solvent removed under reduced pressure to yield a pale yellow oil. Purification by vacuum distillation (80−84 °C, 0.20 Torr) yielded the product as a clear colorless oil (1.97 g, 57%): ^{1}H NMR ($CDCl_3$, 300 MHz) δ 2.85 (heptet, J = 6.6 Hz, 1H), 2.73 (s, 4H), 2.67 (m, 4H), 2.52 (m, 4H), 2.10 (br, 2H), 0.99 (d, J = 6.6 Hz, 6H) ppm; HREIMS calcd for $C_9H_{21}N_3$ 171.1735, found 171.1737. Anal. Calcd for $C_9H_{21}N_3$: C, 63.09; H, 12.36; N, 24.54. Found: C, 61.81; H, 12.33; N, 24.05.

1,4-bis(2-hydroxy-3,5-di-*tert*-butylbenzyl)-7-isopropyl-1,4,7-triazacyclononane ($H_2L^{tBu_4}$). To a solution of 1-isopropyl-1,4,7-triazacyclononane (0.300 g, 1.75 mmol) in MeOH (5 rnL) was added 37% aqueous formaldehyde (0.355 g, 4.38 mmol). This solution was refluxed under N_2 for 3 h. A solution of 2,4-di-*tert*-butylphenol (0.753g, 3.65 mmol) in MeOH (2 mL) was then added. The resulting solution was refluxed for an additional 14 h. Upon cooling the solution to room temperature, a white precipitate began to form. Addition of 5 mL of H_2O to the light yellow solution induced the precipitation of an additional amount of white solid. After the supernatant was decanted away, the solid was dissolved in Et_2O (20 mL) and washed with 3 M NaOH (15 mL). The Et_2O layer was removed and dried over $MgSO_4$, and the solvent was then evaporated under reduced pressure to yield the product as a white solid (0.732 g, 69%): ^{1}H NMR (300 MHz, $CDCl_3$) δ 10.44−11.31 (br, 2H), 7.19 (d, J = 2.4 Hz, 2H), 6.77 (d, J = 2.1 Hz, 2H), 3.73 (s, 4H), 3.02 (s, 4H), 2.93 (heptet, J = 6.6 Hz, 1H), 2.71 (m, br, 4H), 2.59 (m, br, 4H), 1.41 (s, 18H), 1.25 (s, 18H), 0.96 (d, J = 6.6 Hz, 6H) ppm; HRCIMS calcd for $C_{39}H_{65}N_3O_2$ 607.5076, found 607.5063. Anal Calcd. for $C_{39}H_{65}N_3O_2$: C, 77.05; H, 10.78; N, 6.91. Found: C, 76.09; H, 10.61; N, 6.65.

General Method for the Preparation of the Complexes $L^{RR'}MCl$ (M = Cu or Zn). A solution of $L^{RR'}$ (typically 0.15 g) in THF (3 rnL) was treated with excess NaH, causing the evolution of H_2; stirring was continued until gas evolution ceased. The mixture was then filtered, and the filtrate treated with solid anhydrous MCl_2 (M = Cu or Zn, 1.0 equiv), in the case of M = Cu causing the development of a deep purple color. After stirring for 2 h, the mixture was filtered through a pad of Celite and the filtrate evaporated to dryness. Recrystallization by diffusion of pentane into a solution of the complex in CH_2Cl_2/toluene (1:2) yielded the $L^{RR'}MCl$ complexes as purple (M = Cu) or colorless (M = Zn) crystalline solids in the yields noted.

$L^{Me_2}CuCl$ (70% yield): EPR (1:1 CH_2Cl_2/toluene, 77 K, 9.46 GHz) $g_{\|} = 2.25$, $A_{\|} = 160 \times 10^{-4}$ cm^{-1}, $g_{\perp} = 2.03$; FAB-MS (MNBA) *m/z* 444 [M^+]. Anal. Calcd for $C_{21}H_{36}N_3OCuCl\cdot 0.5\ H_2O$: C, 55.49; H, 8.20; N, 9.43. Found: C, 55.50; H, 7.87, N, 9.20.

$L^{tBu_2}CuCl$ (86% yield): EPR (1:1 CH_2Cl_2/toluene, 77 K, 9.46 GHz) $g_{\|} = 2.26$, $A_{\|} = 161 \times 10^{-4}$ cm^{-1}, $g_{\perp} = 2.04$. Anal. Calcd for $C_{27}H_{48}N_3OCuCl$: C, 61.22; H, 9.13; N, 7.93. Found: C, 60.85; H, 8.96; N, 7.90.

$L^{MeOMe}CuCl$ (87% yield): EPR (1:1 CH_2Cl_2/toluene, 77 K, 9.46 GHz) $g_{\|} = 2.26$, $A_{\|} = 158 \times 10^{-4}$ cm^{-1}, $g_{\perp} = 2.02$. Anal. Calcd for $C_{21}H_{36}N_3O_2CuCl\cdot 0.5\ CH_2Cl_2$: C, 51.24; H, 7.40; N, 8.34. Found: C, 51.12; H, 7.50; N, 8.05.

$L^{tBuSMe}CuCl\cdot H_2O$ (72% yield): EPR (1:1 CH_2Cl_2/toluene, 77 K, 9.46 GHz) $g_{\|} = 2.26$, $A_{\|} = 157 \times 10^{-4}$ cm^{-1}, $g_{\perp} = 2.06$. Anal. Calcd for $C_{24}H_{42}N_3OSCuCl\cdot H_2O$: C, 53.71; H, 8.27; N, 7.83. Found: C, 54.12; H, 7.83; N, 7.74.

$L^{Me_2}ZnCl$ (60% yield): ^{1}H NMR (300 MHz, $CDCl_3$) δ 6.81 (d, J = 1.5 Hz, 1H), 6.52 (d, J = 1.5 Hz, 1H), 3.90−3.74 (overlapping singlet and heptet, 4H), 3.16−3.05 (m, 2), 2.75−2.60 (m, 6H), 2.60−2.50 (m, 2H), 2.35−2.25 (m, 2H), 2.19 (s, 3H), 2.12 (s, 3H), 1.18 (d, J = 6.6 Hz, 6H), 0.98 (d, J = 6.6 Hz, 6H) ppm. Anal. Calcd for $C_{21}H_{36}N_3OClZn\cdot 0.5\ H_2O$: C, 55.27; H, 8.17; N, 9.21. Found: C, 55.01; H, 7.88; N, 9.24.

$L^{tBu_2}ZnCl$ (96% yield): ^{1}H NMR (300 MHz, CD_2Cl_2) δ 7.20 (d, J = 2.4 Hz, 1H), 6.80 (d, J = 2.4 Hz, 1H), 3.89 (heptet, J = 6.6 Hz, 2H), 3.81 (s, 2H), 3.25−3.23 (m, 2H), 2.98−2.93 (m, 2H), 2.71−2.64 (m, 6H), 2.48−2.41 (m, 2H), 1.86 (br., 2H, H_2O), 1.49 (s, 9H), 1.29 (s, 9H), 1.18 (d, J = 6.6 Hz, 6H), 1.12 (d, J = 6.6 Hz, 6H) ppm. Anal. Calcd for $C_{27}H_{48}N_3OClZn\cdot H_2O$: C, 59.01; H, 9.17; N, 7.65. Found: C, 59.10; H, 9.17; N, 7.65.

$L^{tBuSMe}ZnCl$ (93% yield): ^{1}H NMR (500 MHz, $CDCl_3$) δ 7.07 (d, J = 2.0 Hz, 1H), 6.71 (d, J = 2.0 Hz, 1H), 3.88 (heptet, J = 6.5 Hz, 2H), 3.82 (s, 2H), 3.18 (m, br, 2H), 2.74 (m, br, 4H), 2.72 (m, br, 2H), 2.59 (m, br, 2H), 2.43 (s, 3H), 2.35 (m, br, 2H), 1.26 (s, 9H), 1.24 (d, J = 6.5 Hz, 6H), 1.05 (d, J = 6.5 Hz, 6H) ppm. Anal. Calcd for $C_{24}H_{42}N_3OSZnCl$: C, 55.47; H, 8.15; N, 8.09. Found: C, 55.29; H, 8.14; N, 8.12.

General Method for the Preparation of the Complexes $L^{RR'}Cu(O_2CCH_3)$. These complexes were prepared in a fashion similar to that of $L^{RR'}CuCl$, substituting anhydrous $Cu(O_2CCH_3)_2$. Recrystallization by pentane diffusion into solutions of the complexes in CH_2Cl_2/toluene (1:2) yielded the $L^{RR'}Cu(O_2CCH_3)$ complexes as brown or green crystalline solids in the yields noted.

$L^{tBu_2}Cu(O_2CCH_3)$ (65% yield): EPR (1:1 CH_2Cl_2/toluene, 77 K, 9.46 GHz) $g_{\|} = 2.26$, $A_{\|} = 175 \times 10^{-4}$ cm^{-1}, $g_{\perp} = 2.03$; FAB-MS (MNBA) m/z 552 [M^+].

$L^{MeOMe}Cu(O_2CCH_3)\cdot CH_2Cl_2$ (85% yield): EPR (1:1 CH_2Cl_2/toluene, 77 K, 9.46 GHz) $g_{\|} = 2.27$, $A_{\|} = 167 \times 10^{-4}$ cm^{-1}, $g_{\perp} = 2.04$. Anal. Calcd for $C_{24}H_{41}N_3O_4Cl_2Cu$: C, 50.57; H, 7.23; N, 7.37. Found: C, 50.57; H, 7.12; N, 7.33.

$L^{MeSMe}Cu(O_2CCH_3)\cdot CH_2Cl_2$ (75% yield): EPR (1:1 CH_2Cl_2/toluene, 77 K, 9.46 GHz) $g_{\|} = 2.27$, $A_{\|} = 166 \times 10^{-4}$ cm^{-1}, $g_{\perp} = 2.02$. Anal. Calcd for $C_{24}H_{41}N_3O_3SCl_2Cu$: C, 49.18; H, 7.05; N, 7.17. Found: C, 49.81; H, 6.84; N, 7.20.

$[L^{tBu_2}Cu(CH_3CN)]CF_3SO_3$. To a solution of Na[$L^{tBu_2}$] in THF (5 mL), prepared by treatment of L^{tBu_2} (0.319 g, 0.74 mmol) with excess NaH followed by filtration, was added a solution of $Cu(CF_3SO_3)_2$ (0.262 g, 0.72 mmol) dissolved in CH_3CN (1 mL), causing a color change to deep purple. After stirring for 30 min, the solvent was removed under reduced pressure, and the resultant purple residue redissolved in CH_2Cl_2 (5 mL) and filtered through Celite, and the filtrate evaporated. Recrystallization of the purple solid from a mixture of CH_3CN/toluene/pentane (1:5:10) at −20 °C for 5−7 days afforded the pure product as purple crystals (0.45 g, 93%): EPR (1:1:0.1 CH_2Cl_2/toluene/CH_3CN, 77 K, 9.46 GHz) $g_{\|} = 2.25$, $A_{\|} = 160 \times 10^{-4}$ cm^{-1}, $g_{\perp} = 2.03$; ISP-MS (CH_2Cl_2) *m/z* 493 [$M - CH_3CN - CF_3SO_3^+$]. Anal. Calcd for $C_{30}H_{51}N_4O_4F_3SCu$: C, 52.65; H, 7.51; N, 8.19. Found: C, 52.21; H, 7.51; N, 8.31.

$L^{tBu_4}M\cdot MeOH$. To a solution of $H_2L^{tBu_4}$ (0.300 g, 0.493 mmol) in THF (5 mL) under nitrogen was added excess NaH (0.048 g, 2.00 mmol). The resultant mixture was stirred until H_2 evolution ceased (2 h). The light yellow solution was filtered through a pad of Celite, and the filtrate was treated with a THF suspension (4 mL) of anhydrous MCl_2 (M = Cu or Zn, 1 equiv). This caused the formation of a murky green (M = Cu) or light yellow (M = Zn) solution which was stirred overnight at ambient temperature. The solution was then filtered through a pad of Celite and the THF removed under reduced pressure.

The green powder obtained was recrystallized by slow evaporation of a MeOH/H_2O (70:30) solution over the course of 3 days, yielding dark green (M = Cu) or light yellow (M = Zn) crystals.

$L^{tBu_4}Cu\cdot MeOH$ (54% yield): EPR (1:1 CH_2Cl_2/toluene, 77 K, 9.46 GHz) $g_{\|} = 2.25$, $A_{\|} = 169 \times 10^{-4}$ cm^{-1}, $g_{\perp} = 2.03$; FAB-MS (MNBA) *m/e* 669 (M^+, 100). Anal. Calcd for $C_{39}H_{63}N_3O_2Cu\cdot CH_3OH$: C, 68.48; H, 9.63; N, 5.99. Found: C, 68.52; H, 9.67; N, 6.12.

$L^{tBu_4}Zn\cdot MeOH$ (56% yield): ^{1}H NMR (500 MHz, $CDCl_3$) δ 7.22 (d, $J = 2.5$ Hz, 2H), 6.78 (d, $J = 2.5$ Hz, 2H), 4.58 (d, $J = 11.5$ Hz, 2H), 3.46 (s, 3H), 3.39 (d, $J = 11.5$ Hz, 2H), 3.38 (heptet, $J = 6.5$ Hz, 1H), 3.11 (m, br, 2H), 2.80 (m, br, 4H), 2.51 (m, br, 4H), 2.33 (m, br, 2H), 1.51 (s, 18H), 1.27 (s, 18H), 0.84 (d, $J = 6.5$ Hz, 6H) ppm. Anal. Calcd for $C_{39}H_{63}N_3O_2Zn\cdot CH_3OH$: C, 68.31; H, 9.60; N, 5.97. Found: C, 68.58; H, 9.55; N, 5.92.

Coulometric oxidations of $[L^{tBu_2}Cu(CH_3CN)]CF_3SO_3$ and $L^{tBu_4}Cu$. A three-chamber electrochemical cell was charged with a solution of $[L^{tBu_2}Cu(CH_3CN)]CF_3SO_3$ (0.0045 g, 7.0×10^{-3} mmol) or $L^{tBu_4}Cu\cdot$MeOH (0.0062 g, 8.8×10^{-3} mmol) in CH_2Cl_2 (0.4 M $TBAPF_6$), fitted with a platinum gauze working electrode, a silver wire pseudoreference electrode, and a platinum wire auxiliary electrode, and then cooled to −40 °C under an atmosphere of dry N_2. Coulometric oxidation was then performed at 1.0 V (L^{tBu_2} complex) or 0.71 V (L^{tBu_4} complex), resulting in the removal of 0.8 ± 0.1 e$^-$ mol^{-1} (L^{tBu_2}) or 1.0 ± 0.1 e$^-$ mol^{-1} (L^{tBu_4}) of the compound and a color change to deep green (L^{tBu_2}) or dark blue (L^{tBu_4}). For the L^{tBu_2} case, an aliquot of the green solution was removed by syringe and transferred to a precooled EPR tube, and the X-band EPR spectrum subsequently recorded at 77 K. Analysis revealed the presence of a residual axial Cu(II) signal superimposed on a weak isotropic signal at $g = 2.00$; double integration of the entire signal revealed a 92 ± 5% decrease in the signal intensity compared to that of the original sample. Concurrent UV−vis analysis of the green solution (−40 °C) revealed the presence of new absorption features with $\lambda_{max} = 410$ ($\epsilon = 3500$ M^{-1} cm^{-1}) and 648 ($\epsilon = 1000$ M^{-1} cm^{-1}) nm.

Chemical Oxidation of $[L^{tBu_2}Cu(CH_3CN)]^+$, $L^{tBu_2}ZnCl$, and $L^{tBu_4}M$ (M = Cu or Zn). Solutions of the M^{II}−phenoxyl radical species derived from these precursors were prepared by treatment with $(NH_4)_2[Ce(NO_3)_6]$ in CH_2Cl_2/CH_3CN or CH_2Cl_2/toluene/CH_3CN mixtures at −40 °C or with [thianthryl]BF_4 in CH_2Cl_2 at −80 °C (see Table 3 and Figures 4, 5, and 7 for spectroscopic data). For example, a solution of $[L^{tBu_2}Cu(CH_3CN)]CF_3SO_3$ (0.013 g, 0.02 mmol) in CH_2Cl_2 (5.0 mL) was cooled to −40 °C under a N_2 atmosphere and treated with a solution of $(NH_4)_2[Ce(NO_3)_6]$ (0.011 g, 0.02 mmol) dissolved in CH_3CN (1.5 mL), causing a color change from purple to deep green. The sample for resonance Raman spectroscopy was produced by treating a solution of $[L^{tBu_2}Cu(CH_3CN)]CF_3SO_3$ (0.026 g, 0.04 mmol) in CD_3CN (2.0 mL) with a solution of $(NH_4)_2[Ce(NO_3)_6]$ (0.022 g, 0.04 mmol) in CD_3CN (1.5 mL) at −40 °C, yielding a final concentration of $[(L^{tBu_2})Cu(CH_3CN)]^{2+}$ of 11.5 mM. Solutions of $[L^{tBu_2}ZnCl]^+$ and $[L^{tBu_4}M]^+$ (M = Cu or Zn) were prepared similarly, except for $[L^{tBu_2}ZnCl]^+$ a 1:4 CH_2Cl_2/toluene solution of $L^{tBu_2}ZnCl$ was used and for $[L^{tBu_4}Zn]^+$ a 1:1 CH_2Cl_2/toluene solution of $L^{tBu_4}Zn$ was used. The solution of $[L^{tBu_4}Cu]^+$ was dark blue, and those of the Zn compounds were light green. EPR data for $[L^{tBu_2}ZnCl]^+$ and $[L^{tBu_4}Zn]^+$ (∼1:1:0.1 CH_2Cl_2/toluene/CH_3CN, 77 K, 9.46 Ghz, field modulation amplitude 1.0 G, microwave power 20 μW): $g_{iso} = 2.00$.

X-ray Crystallography. A purple plate crystal of $[L^{tBu_2}Cu(CH_3CN)]CF_3SO_3\cdot C_7H_8$, a colorless prism of $L^{Me_2}ZnCl\cdot 0.32H_2O$, a yellow block crystal of $L^{tBu_4}Zn\cdot CH_3OH$, and a green brown prismatic crystal of $L^{MeSMe}Cu(O_2CCH_3)\cdot CH_2Cl_2$ were fixed to thin glass fibers with epoxy resin and mounted on an Enraf-Nonius CAD4 diffractometer for data collection at 293(2) K. Cell constants and orientation matrices were determined by least-squares refinement of the setting angles of 25 carefully centered reflections. The intensities of three standard reflections were monitored hourly in order to calculate corrections for decay. For $[L^{tBu_2}Cu(CH_3CN)]CF_3SO_3\cdot C_7H_8$, a 6.9% decrease in the intensities of these reflections was noted, and the data were scaled to adjust for this decay. The data were corrected for Lorentz and polarization effects. Absorption corrections were determined from a series of azimuthal scans of three intense reflections for each complex. Diffraction data for a green-brown plate crystal of $L^{tBu_4}Cu\cdot CH_3OH$ were collected using a Siemens SMART platform CCD diffractometer at 173(2) K. Initial cell constants and an orientation matrix were determined from 60 reflections harvested from 20 frames. Final cell constants were calculated from a set of 8192 strong reflections from the actual data collection. An absorption correction was determined using the program SADABS.[42]

Space group determinations were made on the basis of systematic absences and intensity statistics. The structures were solved by direct methods which provided the positions of most of the non-hydrogen atoms. The remainder of the non-hydrogen atoms were located following several full-matrix least squares/difference Fourier cycles. All non-hydrogen atoms were refined with anisotropic displacement parameters unless noted below. Hydrogen atoms were placed in calculated positions and refined as riding atoms with fixed isotropic displacement parameters [1.2 × host atom *U*(eq) for methylene and methine, 1.5 × host atom *U*(eq) for methyl and hydroxylic protons]. The carbon atoms of the toluene molecule located in the asymmetric unit of $[L^{tBu_2}Cu(CH_3CN)]CF_3SO_3\cdot C_7H_8$ were refined isotropically. Although the carbon atoms of the *tert*-butyl group *para* to the phenolic oxygen atom exhibit large anisotropic displacement parameters, a suitable split atom model could not be determined. A CH_2Cl_2 molecule was located in the asymmetric unit of $L^{MeSMe}Cu(O_2CCH_3)\cdot CH_2Cl_2$, and a partially occupied (0.32) water molecule was identified in the asymmetric unit of $L^{Me_2}ZnCl\cdot 0.32\ H_2O$. Methanol molecules were found to be hydrogen bonded to phenolate oxygens in the asymmetric units of $L^{tBu_4}Cu\cdot CH_3OH$ and $L^{tBu_4}Zn\cdot CH_3OH$. In the latter complex, one *tert*-butyl group was found to be rotationally disordered over two positions in a 50:50 ratio. Bond length restraints were applied to the carbon atoms of the disordered groups.

All calculations were performed using the SHELXTL-Plus V5.0 suite of programs on an SGI INDY R4400-SC computer.[43] Important crystallographic details are summarized in Table 1, and relevant bond lengths and angles are found in Table 2. Full details of the structure determinations, including fractional atomic coordinates, and full tables of bond lengths and angles, anisotropic displacement parameters, torsion angles, and hydrogen atom coordinates are included in the Supporting Information.

Acknowledgment. Funding for this work was provided by the National Institutes of Health (Grant GM47365 to W.B.T., Grant GM33162 to L.Q., a predoctoral traineeship to E.C.W., and a postdoctoral fellowship to L.M.B.), the National Science Foundation (NYI award to W.B.T. and Grant CHE-9413114 for partial support for the purchase of the Siemens SMART system), the University of Minnesota (dissertation fellowship to J.A.H.), and the Alfred P. Sloan and Camille & Henry Dreyfus Foundations (fellowships to W.B.T.).

Supporting Information Available: FTIR and $^{13}C\{^1H\}$ NMR spectral data and complete drawings and full details of the X-ray structure determinations, including tables of bond lengths and angles, atomic positional parameters, and final thermal parameters (87 pages). See any current masthead page for ordering and Internet access instructions.

JA9700663

(42) Blessing, R. H. *Acta Crystallogr.* **1995,** *A51,* 33−38.

(43) SHELXTL V5.0, Siemens Energy & Automation, Inc., Madison, WI 53719-1173.